Catena 241 (2024) 108059

Contents lists available at ScienceDirect

Catena

journal homepage: www.elsevier.com/locate/catena

The last deglaciation in the central Pyrenees: The 47 ka Pllan d'Están paleolake record (Ésera valley)

Ixeia Vidaller [a,*], Ana Moreno [a], Penélope González-Sampériz [a], Sergi Pla-Rabés [b], Alicia Medialdea [c], Miren del Val [c], Juan Ignacio López-Moreno [a], Blas Valero-Garcés [a]

[a] Instituto Pirenaico de Ecología, Consejo Superior de Investigaciones Científicas (IPE-CSIC), Zaragoza, Spain
[b] Unitat d'Ecologia, Department de Biologia Animal, Biología Vegetal i Ecología, Universitat Autonoma de Barcelona, Barcelona, Spain
[c] Centro Nacional de Investigación sobre la Evolución Humana (CENIEH), Burgos, Spain

ARTICLE INFO

Keywords:
Paleolake
Pyrenees
Last Deglaciation
Diatoms
Pollen

ABSTRACT

Last deglaciation was a complex period in southern European mountains with several glacier advances associated to rapid climate changes which differ in terms of timing and intensity. The 46.7 ka BP lacustrine sequence of Pllan d'Están paleolake (1840 m a.s.l.) located in the Central Southern Pyrenees (northern Spain) provides new information about that deglaciation period for the first time in the Ésera valley. We present a multiproxy analysis including sedimentological, geochemical and biological (pollen and diatoms) indicators that, together with a chronological frame constrained by ^{14}C and OSL dates, enabled the longest reconstruction of the glacier evolution, climate and environmental change made in the Pyrenees to date. This lacustrine sedimentary sequence (4.9 m) is composed of banded to finely laminated silts with few intercalations of massive sections where carbonatic, siliciclastic and organic facies appear from the bottom to the top, characterizing environmental changes from a subglacial/proglacial lake to the current peatbog. A cold and glacier dominated period from 46.7 to 15.9 ka BP was interrupted by a warmer period spanning from 38.2 to 34.8 ka BP. The vegetation succession determined by the palynological analyses is similar to other Pyrenean valleys but dates the onset of mesophytes expansion at 13.8 ka BP during the Allerød, pointing to a difference with other European sequences where temperate forest development took place earlier, associated to the Bølling period. The colder conditions of the Younger Dryas (13–11.7 ka BP) have been detected from cold tolerant diatom taxa that preceded a peatbog development during the Holocene (11.7 ka BP – present-day). These results, together with previously studied Pyrenean sequences, allow characterizing past environmental changes during last deglaciation phases in southern Europe.

1. Introduction

Changes in surface area and volume of glaciers are sensitive indicators of climate variability in mountain regions, both during Quaternary times and the current global warming (eg. Beniston et al., 2018; Braithwaite & Hughes, 2020). Nowadays, the southernmost remaining glaciers in Europe are found in the Central Pyrenees (Grunewald and Scheithauer, 2010). Currently, these glaciers are very small (<0.5 km^2; Huss and Fischer, 2016) and, due to the global warming, they are in risk of disappearing in the coming decades (López-Moreno et al., 2016; Vidaller et al., 2023, 2021). However, the glaciers in the central Pyrenees occupied much of the area above 1500 m a.s.l. during the last glacial cycle (ca. 60–11.7 ka BP) (e.g. Oliva et al., 2019), their fronts reached an approximate altitude of 800 m during the maximum extent (Pyrenean Last Glacial Maximum, PLGM, ca. 60 ka BP; Lewis et al., 2009). Three main phases of glacier advance during the Last Glacial Cycle (LGC) have been established for Central Pyrenees: the local maximum extent (PLGM) at ca. 60 ka BP (MIS 4), the 36 ka BP stage (MIS 3) and the last one at 22–17 ka BP partially overlapping the global LGM (MIS 2, LGM) (Bartolomé et al., 2021; Crest et al., 2017; García-Ruiz et al., 2012; Gellatly et al., 1992; González-Sampériz et al., 2017, 2006; Jiménez-Sánchez et al., 2013; Jomelli et al., 2020; Lewis et al.,

* Corresponding author.
E-mail addresses: ixeia@ipe.csic.es (I. Vidaller), amoreno@ipe.csic.es (A. Moreno), pgonzal@ipe.csic.es (P. González-Sampériz), s.pla@creaf.uab.cat (S. Pla-Rabés), alicia.medialdea@cenieh.es (A. Medialdea), miren.delval@cenieh.es (M. del Val), nlopez@ipe.csic.es (J.I. López-Moreno), blas@ipe.csic.es (B. Valero-Garcés).

https://doi.org/10.1016/j.catena.2024.108059
Received 25 September 2023; Received in revised form 25 March 2024; Accepted 22 April 2024
Available online 3 May 2024

2009; Martí-Bono and García-Ruíz, 1994; Morellón et al., 2008; Pallàs et al., 2006; Sancho et al., 2018). Along the Holocene, Pyrenean glaciers have been retreating to the highest cirques, although several advances were recorded (e.g. Neoglacial, cold Iron Age or Little Ice Age) (García-Ruiz et al., 2016; Hughes, 2018; Oliva-Urcía et al., 2018). Recently, Moreno et al., (2021) demonstrated the presence of ice during the Roman and Medieval Climatic Anomaly (MCA) in the Monte Perdido glacier, pointing to a complex history of Pyrenean glaciers including preservation in, at least, some warm periods of the past millennia.

Timing of Pyrenean glacier evolution follows in general terms northern hemisphere climate oscillations, and thus it is in synchrony with other glaciers in Europe. However, some differences have been highlighted in the last decades regarding the timing of maximum glacier extension and the deglaciation process (e.g. Hughes and Woodward, 2008). During the global Last Glacial Maximum (LGM) (23–19 ka BP) there was a general increase in mountain glacier extension (Hughes et al., 2013), however, in the Pyrenees and other Mediterranean regions, the extension reached by the glacial tongues during this period is not well constrained, as moraine deposits are not well identified neither dated (Delmas, 2015; González-Sampériz et al., 2006; Jomelli et al., 2020; Pallàs et al., 2006). Many studies based on dating moraines and associated lake deposits in the Pyrenees indicated that the maximum extent of glaciers during the last glacial cycle occurred earlier than the global LGM, so deglaciation started much earlier than after the global LGM (García-Ruiz et al., 2013; García-Ruiz et al., 2012; Lewis et al., 2009; Oliva et al., 2019). The identified deglaciation history of Pyrenean glaciers after the global LGM shows several events of glacial stabilization synchronous with cold periods as Oldest, Older and Younger Dryas (Bartolomé et al., 2021; Crest et al., 2017; García-Ruiz et al., 2016; Palacios et al., 2017). Unfortunately, the relatively limited number of moraines and polished surfaces that have been dated hinders the compilation of continuous series of glacier evolution (Leonard and Reasoner, 1999) thus eluding a full understanding of last deglaciation complex dynamics in the region.

Lacustrine sediments from Pyrenean lakes have provided a more continuous and detailed record of climate and environmental conditions during the last glacial cycle (e.g. González-Sampériz et al., 2020, 2017, 2006; Leunda et al., 2017; Morellón et al., 2012, 2008; Moreno et al., 2012, 2010; Oliva-Urcía et al., 2018; Pérez-Sanz et al., 2013). In the Central Southern Pyrenees, the Tramacastilla record (García-Ruiz et al., 2003; Jalut et al., 1982; Montserrat Marti, 1992) provided evidence for an early deglaciation in the southern Pyrenees. The Portalet peatbog in the headwaters of the Gállego river (1802 m a.s.l.) represents, until this study, the oldest available high-altitude lacustrine record of glacier evolution with an early deglaciation phase (starting at 36 ka BP) and minor glacier advances during the global LGM and the Younger Dryas (González-Sampériz et al., 2006). Other lake sequences, as Marboré lake sequence (2612 m a.s.l.), in the Cinca valley (Leunda et al., 2017; Oliva-Urcía et al., 2018), Basa de la Mora lake (Pérez-Sanz et al., 2013) and Redon lake (Catalan et al., 2014; Pla and Catalan, 2005), provided a detailed Holocene paleoclimate and vegetation record with some evidences of glacial advance during the Neoglacial.

Unfortunately, there is not much information from the Ésera valley, in the east sector of the Central Pyrenees (Spain) where the largest glaciers occurred during the last glacial cycle. The Ésera valley is currently the most glaciated valley in the Pyrenees (Vidaller et al., 2021) and it developed some of the largest and thickest glaciers during the last Glacial Maximum (García-Ruiz and Serrano, 2022). There are numerous studies about the recent evolution of the Ésera glaciers (Aneto, Maladeta, Tempestades, Barrancs and Coronas glaciers) since the Little Ice Age (LIA), mostly based on current measurements of glacier extension (López-Moreno et al., 2016; Rico et al., 2017; Vidaller et al., 2023). Additionally, the Ésera valley was the subject of several geomorphological studies where Upper Pleistocene moraines and related lake deposits were identified and associated to the main glacial phases (Bordonau, 1993, 1992; Martínez de Pisón, 1990). Later, geomorphological cartographies such as those from Chueca-Cía and Julián-Andrés (2008) and García-Ruiz et al. (1992) completed the identification of glacial forms and deposits, particularly for the late Holocene moraine complexes. More recently, a cosmogenic dating study in the moraines and tills of the Maladeta massif (Crest et al., 2017; Reixach, 2022), provided the timing of the main glacier advances of the Ésera glaciers since their maximum extension. The available lake records as the glaciolacustrine rhythmite sequence of Barrancs lake (2360 m a.s.l.) only span the last 3 ka BP (Copons et al., 1997; Copons and Bordonau, 1997). Therefore, long, continuous and multiproxy lacustrine records to reconstruct the paleoclimate and landscape evolution from the Ésera valley and the Maladeta massif are not yet available.

Here we present a multiproxy study of Pllan d'Están paleolake sedimentary sequence, spanning the last 46.7 ka BP, the longest high-altitude lacustrine record in the Central Pyrenees. The study aims clarifying the climate evolution since the Pyrenean Last Maximum Extent , integrating the Ésera glacier evolution in the well-known regional context. This study reconstructs the paleolimnological history of the Pllan d'Están basin throughout the analyses of sedimentological, geochemical and biological (pollen and diatom) proxies constrained by a robust chronological framework based on the combination of ^{14}C and OSL dates. This study also supports the differences in the timing of the last deglaciation previously observed in other Pyrenean records with the general trend observed in Central and Northern Europe. The Pllan d'Están record provides further evidence of an early, but complex, deglaciation in the Pyrenees, outlines some climatic patterns affecting Mediterranean mountain region of southern Europe and highlights regional deglaciation dynamics that differ from the evolution of northern European regions.

2. Study area and geomorphological regional context

2.1. Geological setting

The Ésera valley is located in the Central Pyrenees (North-East Spain) (Fig. 1a). At the headwaters, the southernmost slope of the valley corresponds with the northern slope of Maladeta massif, which is one of the few areas with the presence of active glaciers and permafrost in the Pyrenees (Serrano et al., 2019), both processes are affected by current global warming. The upper valley is a narrow glacial, U-shaped trough surrounded by some of the highest peaks of the Pyrenees, such as the summits of Aneto (3404 m a.s.l.) and Maladeta (3312 m a.s.l.).

Geologically, the Ésera valley belongs to the Axial Zone of the Pyrenees and represents the contact zone between granites originated during the Variscan orogeny, that crop out in the uppermost sector of the valley and the Devonian and Carboniferous limestone, shale and quartzite, strongly affected by both the Variscan and Alpine orogeny and located at the bottom of the valley (García-Sansegundo et al., 2013; Ríos-Aragüés et al., 2002). The Pllan d'Están paleolake basin sits on Carboniferous limestones and shales (Fig. 1b) and the watershed includes both granite and sedimentary formation.

Current landscape has been mostly modelled by the action of glaciers during the last Pleistocene glacial cycle (Copons and Bordonau, 1997; García-Ruiz et al., 1992; Martínez de Pisón, 1990,1989). Due to the different lithology (granite and limestone) till and moraines of granite composition are easily identified and mapped on limestone and shale bedrock. The upper part of the valley is characterized by sharp ridgetops, shallow and big cirques and lakes. There are still very small glaciers up to 3000 m in the north slope of the Ésera valley, as the Aneto Glacier (41.2 ha in 2022) or the Maladeta Glacier (17.4 ha in 2022), two of the largest glaciers in the Pyrenees (Rico et al., 2017; Vidaller et al., 2023, 2021). The bottom of the Ésera valley presents glacial deposits and erosion forms (as glacial striation and troughs). There are extensive areas affected by karstic processes as lapiaz, sinkholes and polje-like landforms. Waters from the upper part of the Ésera valley are transferred to the Garone watershed through numerous sinkholes and ponors

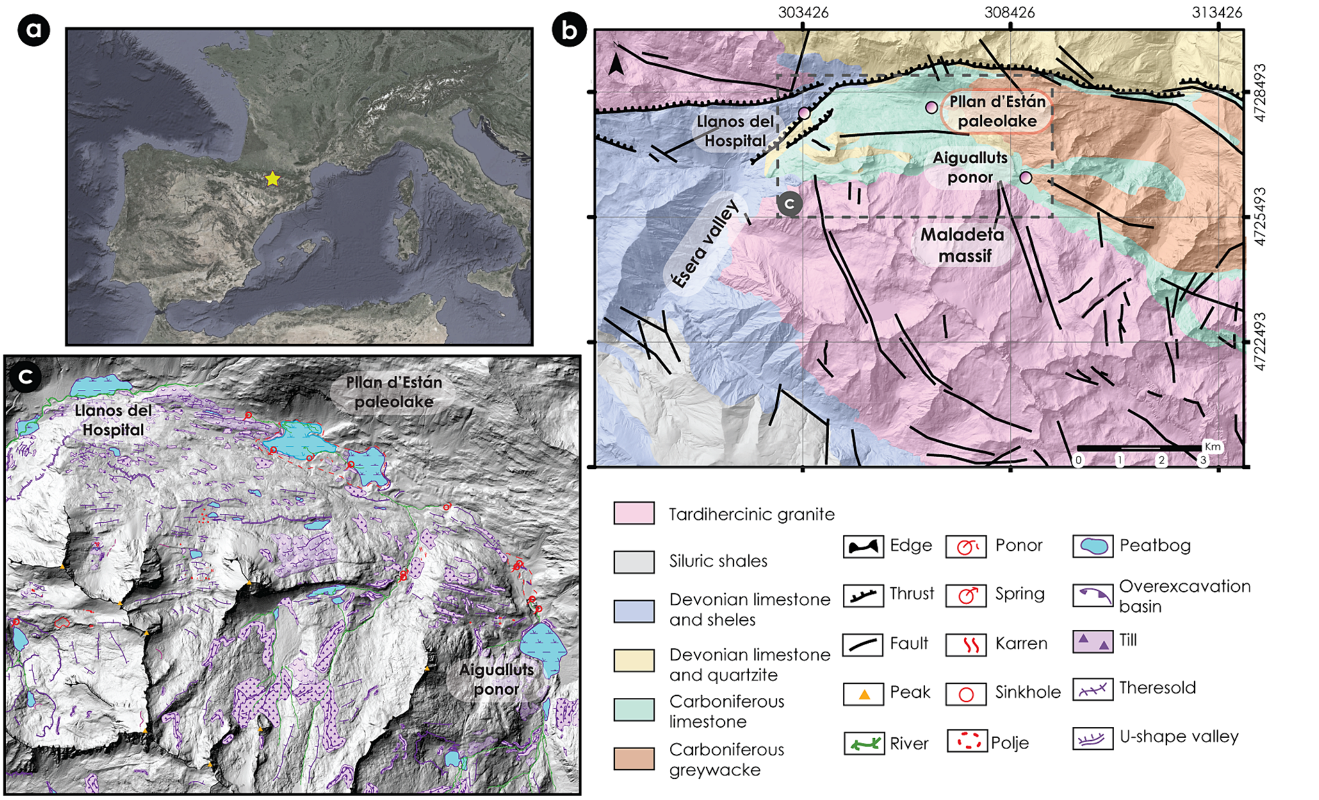

Fig. 1. Location map of Pllan d'Están cores. (a) Location of Pllan d'Están in the south of Europe (Google Earth) Yellow start indicates the location. (b) Simplified geological map of the Maladeta Massif, with the area enlarged in C marked by a black square. (c) Simplified geomorphological map of the surrounding relieves of Pllan d'Están site. (For interpretation of the references to colour in this figure legend, the reader is referred to the web version of this article.)

(Aigualluts) (Chueca-Cía and Julián-Andrés, 2008; García-Ruiz et al., 1992).

Pllan d'Están is a peatbog located at 1840 m a.s.l. within the flooding area of the Ésera river (Fig. 1c), it is in a karstic depression that was reshaped by the passage of the glacier and probably over-excavated. The peatbog area sits on limestone (dominant), quartzite and shales, but granite rocks dominate most of the higher altitude and southern slopes of the watershed. During deglaciation, the glacier supplied water and sediments to the basin, and currently the Ésera river is the main surface inlet and a channel runs through the peatbog. The main outlet is through several ponors at the western end of the basin. Pllan d'Están basin is flooded after heavy rain periods (usually from April to June) and dry during the rest of the year. In winter, from approximately December to April, it is covered by snow (in snowy years the snowpack is more than 2 m thick).

2.2. Climate and vegetation

The Central Pyrenees is a transition region between Mediterranean and Atlantic climate regimes. In this area, the mean annual temperature during 2008–2021 period from the nearest meteorological station (La Renclusa hut, 2140 m a.s.l.) was 4.5 °C. The mean annual precipitation is ~1353 mm/year, mostly occurring in November-December as snow, and in April–May with alternating snow and rainfall events. September/November is a secondary wet period, mainly with rain, although snow events also occur (data from AEMET database).

Pllan d'Están paleolake is located in the subalpine bioclimatic belt, in the Eurosiberian region. Vegetation composition in this area is mainly determined by poor sandy acid soils and dominated by open formations of *Pinus uncinata* with *Rhododendron ferrugineum, Juniperus communis* subsp. *alpine, Vaccinium myrtillus* and *Calluna vulgaris* along with isolated *Sorbus chamaemespilus, Sorbus aucuparia, Salix caprea, Salix bicolor* and *Betula pubescens* as principal trees and shrubs, as well as some patches of *Abies alba* in shady humid locations and *Gymnocarpium dryopteris* as main fern. The vegetation landscape is completed with herbaceous species among which *Deschampia flexuosa* prevail, next to the orchid *Listera cordata* and exceptional endemics such as *Agrostis agrostiflora*, *Campanula latifolia*, *Dianthus barbatus*, *Draba fladnizensis*, *Oxytropis halleri*, *Allium ericetorum*, *Androsace helvetica*, *Saxifraga androsacea* or *Vicia argentea*, between others (Villar et al., 2001).

The traditional livestock activity has led to the deforestation of large areas of the subalpine belt in and around the Ésera valley for their dedication to pastures formed by, depending on the edaphic substrate, *Nardus stricta*, *Trifolium alpinun*, *Meum athamanticun*, *Selinum pyrenaeum*, *Euphorbia cyparissias*, *Gentiana verna*, *Gentiana acaulis*, *Dianthus deltoids*, *Potentilla erecta*, *Nigritella nigra*, *Plantago alpine*, *Festuca rubra*, *Festuca eskia*, *Thymus serpyllum*, *Achillea millefolium*, *Galium caespitosum*, *Campanula ficarioides*, etc. Finally, in streams and wetlands, the hydroseral community is determined by long periods of snow and/or frost conditions and dominant species are *Asplenium septentrionale*, *Cardamine raphanifolia*, *Pinguicula grandiflora*, *Saxifraga aquatica*, *Saxifraga stellaris*, *Carex* sp., *Veratrum álbum*, *Eriophorum latifolium*, *Juncus* sp., *Viola palustris*, *Ranunculus fluviatis*, *Sparganium affine*, *Equisetum* sp. and, sometimes, *Drosera rotundifolia* (Villar et al., 2001).

3. Material and methods

3.1. Field work

Field work to carry out this study comprised geomorphological and geological mapping and sediment coring. The available geomorphological and geological information (Bordonau, 1992; Chueca-Cía and Julián-Andrés, 2008; García-Ruiz et al., 1992; Martínez de Pisón, 1990, 1989; Ollero Ojeda et al., 2001) was compiled and new maps were developed using aerial photographs and field surveys.

Two parallel cores (PDE20-1A-1V and PDE20-1B-1V: Fig. 1c) were retrieved from the western part of Pllan d'Están basin. The site was selected to minimize the impact of the erosion and sedimentation of the river channel in the sediment sequence. Fieldwork was carried out in July 2020 using a *Van Walt/Eijkelkamp* mechanic percussion portable vibracorer. Six drive sections between 70 and 100 cm each, were recovered in each core. The two cores were intercalated (PDE20-1A-1V started at the surface and PDE20-1B-1V started 50 cm under sediment surface) to obtain a complete sequence of 4.9 m.

3.2. Chronology

A total of 30 samples (bulk samples and organic remains) from the master sequence were dated with AMS ^{14}C (see Table 1 in the Section 4.4 *Chronological model*), and 4 OSL (3 IRSL and 1 OSL) dates were obtained from the bottom of core PDE20-1B-1V (Section 6). AMS samples were dated in the Direct AMS laboratory in Seattle (WA, USA). Eleven AMS dates were not included in the final age model as they showed reversals or too young ages (see discussion). Most of these reversals were in the top of the sections where, due to the coring procedure, sediments were mixed and disturbed. Accordingly, we have discarded those intervals.

In order to build the Pllan d'Están depth-age model we used the package 'rbacon' v.3.2.0 (https://cran.r-project.org/web/packages/rbacon/rbacon.pdf) implemented in R (CRAN, Blaauw and Christen (2011). 'rbacon' simultaneously calibrates the input dates (Table) using IntCal20 (Reimer et al., 2020) and builds a Bayesian depth-age model. rbacon employs a gamma autoregressive semi-parametric model to regulate core accumulation rates, accommodating an arbitrary number of subdivisions across the sediment. As in any Bayesian inference, there is a number of prior parameters that in the case of sediment cores are the evolution and shape (α) of accumulation rates, which acts as a factor for the smoothness of the age series. Subsequently, a self-adjusting process is initiated to construct a robust age model resilient to outliers. This involves an adaptive algorithm, in this case Markov Chain Monte Carlo (MCMC), to estimate posterior distributions. Consequently, the model inherently acknowledges the variability in accumulation rates across different sections of a sequence. This implies that minimal variation in accumulation rates within the deposit indicates a heightened "memory" or internal dependence among sequence sections. Hence, this procedure requires specifying the anticipated mean accumulation rate (β) and the prior for the accumulation rate's variability or "memory." Additionally, determining the number of core sections for which the MCMC process will be reiterated is essential. Our prior values for each parameter can be found in the open workflow (https://doi.org/10.5281/zenodo.10839531). We have chosen a Bayesian approach because it provides the most flexible age-depth modelling strategy in archives where sedimentation rates frequently change, several dating methods are used or both. In addition, in the context of lake or paleolake sequences, the deposition rate can be expressed at each depth as a weighted average of preceding depths (Blaauw and Christen, 2011).

The OSL procedures were carried out at the CENIEH in Burgos (Spain). Quartz grains of sizes 90–180 µm were only found in sample LM2021042-01 (the deepest sample). Polymineral fine grains, 4–11 µm, were extracted from each of the three samples and treated with HCl and H_2O_2 to remove carbonate and organic matter, respectively. The polymineral fraction includes both quartz and feldspar grains, with the later dominating the luminescence signal and preventing the detection of the quartz emission. Therefore, the accumulated dose of the fine grain

Table 1
List of the AMS $_{14}C$ and OSL dates obtained in PDE lake. Dates with ID numbers are the dates used to generate the master sequence. The other dates are discarded since they represent sediment that is not in place or has been mixed/disrupted due to coring procedures.

Lab ID	ID	Sample	Type of material	^{14}C age	Calendar age (cal) BP	Composite depth (cm)
D-AMS 041082	**1**	**PDE20-1A-1V-1 10 cm**	Sediment (bulk)	172 ± 29	182 ± 46	10
D-AMS 041083	**2**	**PDE20-1A-1V-1 48 cm**	Sediment (bulk)	5781 ± 26	6576.5 ± 78.5	48
D-AMS 040204	**—**	**PDE20-1A-1V-1 55–57 cm**	Plants remains	——	——	—
D-AMS 040205	**3**	**PDE20-1A-1V-1 76 cm**	Wood	7152 ± 31	7975.5 ± 43.5	76
D-AMS 042372	**—**	**PDE20-1A-1V-2 8–9 cm**	Sediment (bulk)	7775 ± 42	8565.5 ± 29.5	—
D-AMS 040206	**—**	**PDE20-1A-1V-2 25–27 cm**	Plants remains	7319 ± 34	8105 ± 77	—
D-AMS 040203	**5**	**PDE20-1A-1V-2 32–33 cm**	Plants remains	10008 ± 45	11463 ± 189	111
D-AMS 040209	**7**	**PDE20-1A-1V-2 82–84 cm**	Sediment (bulk)	11922 ± 50	13799.5 ± 72.5	162
D-AMS 040210	**—**	**PDE20-1A-1V-3 18–19 cm**	Sediment (bulk)	9539 ± 37	10794 ± 97	—
D-AMS 041724	**—**	**PDE20-1A-1V-3–93-94 cm**	Sediment (bulk)	14646 ± 50	17980 ± 190	—
D-AMS 040211	**—**	**PDE20-1A-1V-4 9 cm**	Sediment (bulk)	9300 ± 36	10477.5 ± 106.5	—
D-AMS 042373	**10**	**PDE20-1A-1V-4 42–43 cm**	Sediment (bulk)	14194 ± 46	17236 ± 150	242
D-AMS 042374	**12**	**PDE20-1A-1V-5 41 cm**	Sediment (bulk)	17990 ± 75	21902 ± 227	303
D-AMS 040212	**14**	**PDE20-1A-1V-5 76–77 cm**	Sediment (bulk)	19555 ± 70	23556.5 ± 234.5	338
D-AMS 042375	**16**	**PDE20-1A-1V-5 94 cm**	Sediment (bulk)	25631 ± 137	29841.5 ± 339.5	356
D-AMS 041725	**17**	**PDE20-1A-1V-6–9-10 cm**	Sediment (bulk)	29646 ± 129	34191 ± 274	370
D-AMS 041091	**19**	**PDE20-1A-1V-6 70 cm**	Sediment (bulk)	33344 ± 189	38232 ± 825	430
D-AMS 041084	**—**	**PDE20-1B-1V-1 8 cm**	Sediment (bulk)	5926 ± 35	6732.5 ± 68.5	—
D-AMS 040207	**4**	**PDE20-1B-1V-1 38–40 cm**	Plants remains	9086 ± 35	10240.5 ± 53.5	77
D-AMS 040208	**6**	**PDE20-1B-1V-1 75–77 cm**	Plants remains	10100 ± 37	11711.5 ± 115.5	115
D-AMS 041085	**—**	**PDE20-1B-1V-1 77 cm**	Sediment (bulk)	9696 ± 35	11144 ± 72	—
D-AMS 041086	**—**	**PDE20-1B-1V-2 10 cm**	Sediment (bulk)	9326 ± 33	10540.5 ± 59.5	—
D-AMS 041087	**8**	**PDE20-1B-1V-2 77 cm**	Sediment (bulk)	12621 ± 43	15039.5 ± 163.5	193
D-AMS 040213	**—**	**PDE20-1B-1V-3 5 cm**	Sediment (bulk)	9565 ± 37	10911.5 ± 185.5	—
D-AMS 041088	**9**	**PDE20-1B-1V-3 47 cm**	Sediment (bulk)	13227 ± 41	15877 ± 151	207
D-AMS 040214	**11**	**PDE20-1B-1V-4 49 cm**	Sediment (bulk)	15989 ± 57	19304.5 ± 170.5	276
D-AMS 041089	**13**	**PDE20-1B-1V-4 77 cm**	Sediment (bulk)	18592 ± 73	22568.5 ± 228.5	304
D-AMS 041726	**15**	**PDE20-1B-1V-5–34 cm**	Sediment (bulk)	22018 ± 86	26201 ± 227	350
D-AMS 042376	**—**	**PDE20-1B-1V-5 52–53 cm**	Sediment (bulk)	24364 ± 130	28529 ± 405	—
D-AMS 041090	**18**	**PDE20-1B-1V-5 76 cm**	Sediment (bulk)	30341 ± 126	34803.5 ± 362.5	393

Lab ID	ID	Sample	Type of material	Type of date	Age (ka BP)	Depth
LM2021042-01	—	**PDE20-1B-1V-6 40–60 cm**	4–11 µm Polymineral fine grain	IRSL	108.7±7.3	488
LM2021042-01	**22**	**PDE20-1B-1V-6 40–60 cm**	90–180 µm Quartz grains	OSL	74.9±7.3	488
LM2021042-02	**21**	**PDE20-1B-1V-6 20–40 cm**	4–11 µm Polymineral fine grain	IRSL	46.7±2.9	455
LM2021042-03	**20**	**PDE20-1B-1V-6 0–20 cm**	4–11 µm Polymineral fine grain	IRSL	34.7±2.2	389

fraction has been estimated through the infrared stimulated luminescence (IRSL) signal of feldspar. In addition, the optically stimulated luminescence (OSL) signal of quartz grains of sample LM2021042-01 was also analysed (more information in *Supplementary Material*).

3.3. Sedimentological and geochemical analysis

The cores were opened, photographed, and sampled at the Pyrenean Institute of Ecology (IPE-CSIC). Photos of each section were taken with a GEOTEK Digital Core Imaging system. Also, magnetic susceptibility (MS) was measured every centimetre with a high-resolution point sensor of a standard GEOTEK multisensory core logger (MSCL-S). Results were reported as instrumental units. For sedimentological analysis and facies description more than 100 smear slides were prepared and observed in an optical microscope, following the method proposed by Schnurrenberger et al. (2003).

X-ray fluorescence (XRF) analyses were performed with an AVAATECH XRF II core scanner at the CORELAB laboratory in the University of Barcelona, with a resolution of 0.5 cm. The analyses were done at 10 kV, 600 micro amperes, 10 s-time span and no filter for Al, Si, P, S, Cl, K, Ca, Ti, V, Cr, Mn, Fe, Rh and Ba; and at 30 kV, 1100 micro amperes, 40 s time span and no filter for Ni, Cu, Zn, Ga, Br, Rb, Sr, Y, Zr, Nb, Mo, Ag, Au, Hg and Pb. Element concentrations are not directly available by the XRF measurements; data were expressed in counts per second (cps). Only elements with higher cps were included in the study: Al, Si, K, Ca, Ti, Fe, Zn, Rb, Sr, Y and Zr. Also, there were obtained the ratio of the intensities of incoherent and coherent scattering (Incoh/Coh).

Total carbon (TC), total nitrogen (TN) and total sulphur (TS) percentages were calculated in the IPE-CSIC laboratory by infrared absorption of CO_2 liberated by combustion in a LECO SC144DR analyser. Total organic carbon (TOC) was calculated considering total inorganic carbon (TIC) and TC (TOC = TC-TIC). Carbonates were only abundant at the bottom section, so TIC was only analysed in the last section of both cores.

A 4.9 m long master composite sequence was obtained combining both cores. The correlation between the two cores (PDE20-1A-1V and PDE20-1B-1V) was made considering the facies description, the presence of characteristic lamination, ^{14}C AMS and OSL dates and geochemical analysis (K and Ca, as representative elements of main compositional variations, Fig. 2).

The statistical analysis of this dataset was made with the software PAST (*v 3.17*; Hammer et al., 2001). This evaluation was made with principal component analyses (PCA) with the obtained data (XRF elements, TIC, TOC, TS and TN), a total of 221 cases and 17 variables. All the variables were linearly interpolated with a regular spacing of 0.5 cm in order to retain the maximum information from the XRF and were normalised to avoid problems arising from their different orders of magnitude.

3.4. Paleobiological analyses

A total of 21 palynological samples were taken along the master sequence, prioritizing the intervals where a valid ^{14}C AMS date was available. Preparation of pollen samples was made at the IPE-CSIC in Zaragoza, following the classic chemical method (Moore et al., 1991), modified and using Thoulet (Goeury and De Beaulieu, 1979) and *Lycopodium clavatum* tablets (Stockmarr, 1971) to test possible sterility of the sediment not associated to the chemical treatment. Pollen sum media was higher than 300 terrestrial grains by sample and the taxa number reached a variety of 90, including hygro-hydrophytes and ferns, despite they were excluded for the total pollen sum and then, for percentages calculation. The pollen diagrams have been drawn using PSIMPOLL (Bennett, 2002) while zonation results following main vegetation changes. Note that this zonation mostly fits with sedimentary units.

Diatoms were only present in the upper 2 m of the master sequence. A total of 24 samples, at 10 cm intervals were selected, treated with 33 % hydrogen peroxide (H_2O_2) and mounted in Naphrax (R.I. = 1.7) following the method described in (Battarbee et al., 2001). At least 300 diatoms valves were counted per sample (mean = 354 valves per sample) under oil immersion at 1000× magnification using differential interference contrast (DIC). Diatom identification was based mainly on Krammer and Lange-Bertalot (1991a,1988,1991b,1986), and Rivera

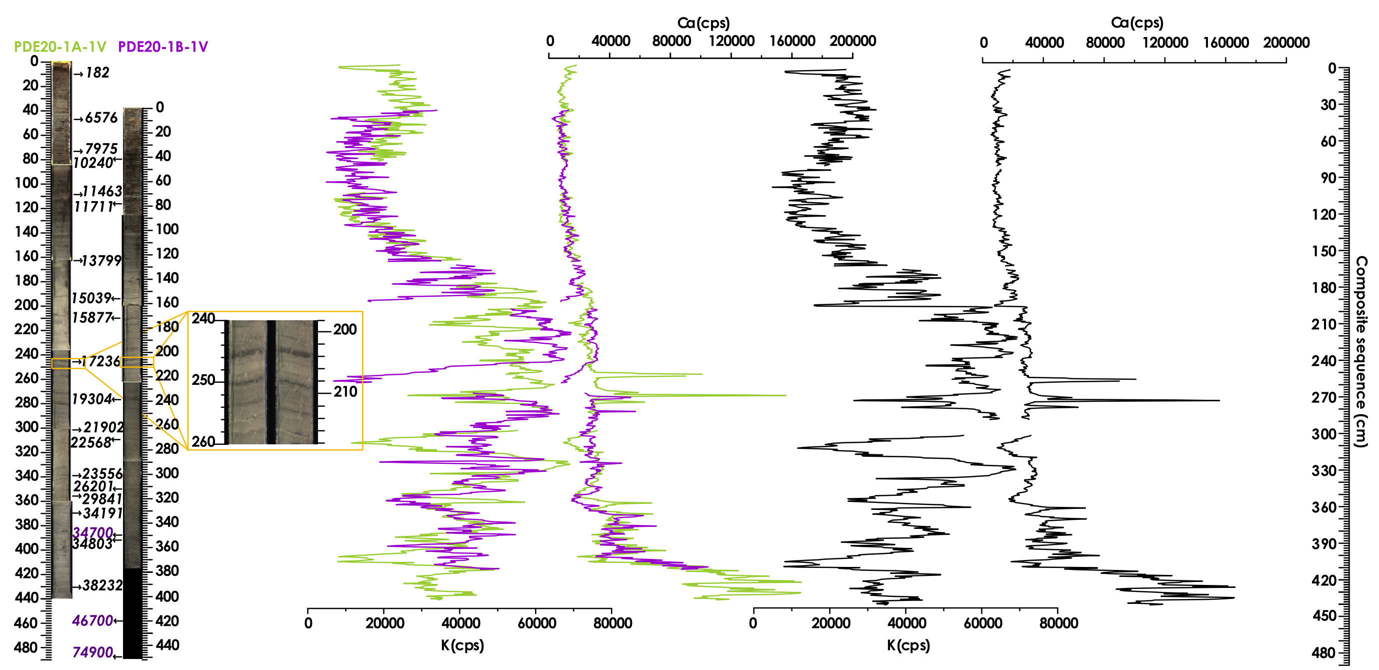

Fig. 2. Correlation between two cores. From left to right: pictures of the two sediment cores, correlation between Ca and K values in both cores and final Ca and K record in the master sequence. Green colour corresponds to PDE20-1A-1V and pink to PDE20-1B-1V. Numbers between sediments cores indicate obtained age results, purple dates corresponds to OSL dates and black dates to AMS ^{14}C. Note that last section of core PDE20-1B-1V is not photographed or scanned for XRF analyses since it was used for OSL dates and it appears in black. See Table 1 in the Section 4.4 *Chronological model*. (For interpretation of the references to colour in this figure legend, the reader is referred to the web version of this article.)

Rondón and Catalan (2017), but basionyms were updated to accepted names following current nomenclature in algae base (https://www.algaebase.org). A PCA using the Hellinger transformation was used to reveal changes in the diatom assemblages' structure through time (Legendre and Gallagher, 2001). Diatoms zones were assessed using time constrained hierarchical clustering CONISS implemented in the R library "Rioja 1.0–5" (Juggins, 2017).

4. Results

4.1. Chronological model

To construct a robust chronological framework of Pllan d'Están paleolake sequence a number of ^{14}C AMS dates were rejected as they not meet stratigraphic, depositional or chronological criteria. Six samples were rejected (Table) since they gave reversal ages once constructed the composite sequence. In addition, four samples provided incoherent ages – too young or too old - and were also discarded to construct the chronology of the master sequence. One submitted sample (D-AMS041083) did not have enough carbon to date it. In the case of the OSL dates, the age derived from IRSL measurements for LM2023042-01 sample, was discarder because of potentially affected by incomplete bleaching. The OSL derived age (see *Supplementary Material*) was used instead.

Finally, the age model was constructed using 19 ^{14}C AMS dates and 3 OSL dates (Fig. 3). Lower sediments, composed by granite till were dated at 74.9 ka BP and were overlain by lacustrine sediments. A possible hiatus separated till sediments from lacustrine deposit, being the first date that indicate lacustrine sedimentation at 46.7 ka BP. The sedimentation rate (SR) of these first lacustrine sediments was generally low (Fig. 3), with an interval of even lower SR between 35 and 23 ka BP (2.5 cm/ka). These two phases with very low SR (450–340 cm depth) are separated by an interval with higher SR, (14.8 cm/ka) that approximately corresponds with the global LGM period. The highest SR of the sequence occurred during last deglaciation (21–12 ka BP) (18.4 cm/ka), until the onset of the Holocene (115 cm depth). During the Holocene, SR slightly decreased to 13.7 cm/ka. There was a hiatus at the top of the sequence between 48 cm (6576 cal BP) and 20 cm (182 cal BP).

4.2. Magnetic susceptibility

The Pllan d'Están sedimentary sequence is composed by fine till at the base (490–450 cm), overlain by banded to finely laminated siliciclastic silt with few intercalations of massive sections (450–150 cm depth) and topped by more organic-rich silts (upper 150 cm). The MS profile show generally low values (8-28x10^{-5}SI), higher in the till and siliciclastic silts and lower in the organic-rich sediments. The upper 70 cm show relatively higher values (Fig. 4).

4.3. Organic and inorganic carbon, total nitrogen and total sulphur content

Total Organic Content (TOC), Total Nitrogen (TN) and Total Sulphur (TS) show similar profiles: low (close to zero) values in the lower sections (450–160 cm), increasing values up to 120 cm with the highest values in the interval 120–60 cm, followed by decreasing and lower values between 60 and 20 cm and relatively higher in the upper 20 cm (Fig. 4). In the lower sections, there were a few intervals with TOC, TN and TS small peaks at 375 and 220–300 cm indicative of some organic matter accumulation. Due to the low TOC values in the lower sections, the TOC/TN ratios are not reliable, except on the sections with some organic matter (375, 220–300 cm depth) where TOC/TN values below 10 appear suggestive of dominant algal contribution. The upper section has three intervals with higher TOC/N values at 175, 100 and 70 cm, suggestive of higher terrestrial organic matter input. The interval with the lowest TOC/N values in the upper 150 cm occurs with the highest TOC values (80–100 cm) pointing to the highest algal organic matter contribution (Meyers, 1997).

Carbonates (indicated by TIC percentages) are absent in the sequence except the lower 360–450 cm interval. Maximum values occur at the base (420–450 cm depth) and decrease upwards. Detrital calcite particles transported by runoff are thus preserved in the oldest sediments associated to the erosion of limestone in the surroundings of the lake (Fig. 1).

4.4. X-ray scanner fluorescence

XRF elements of Pllan d'Están sediments can be divided in three

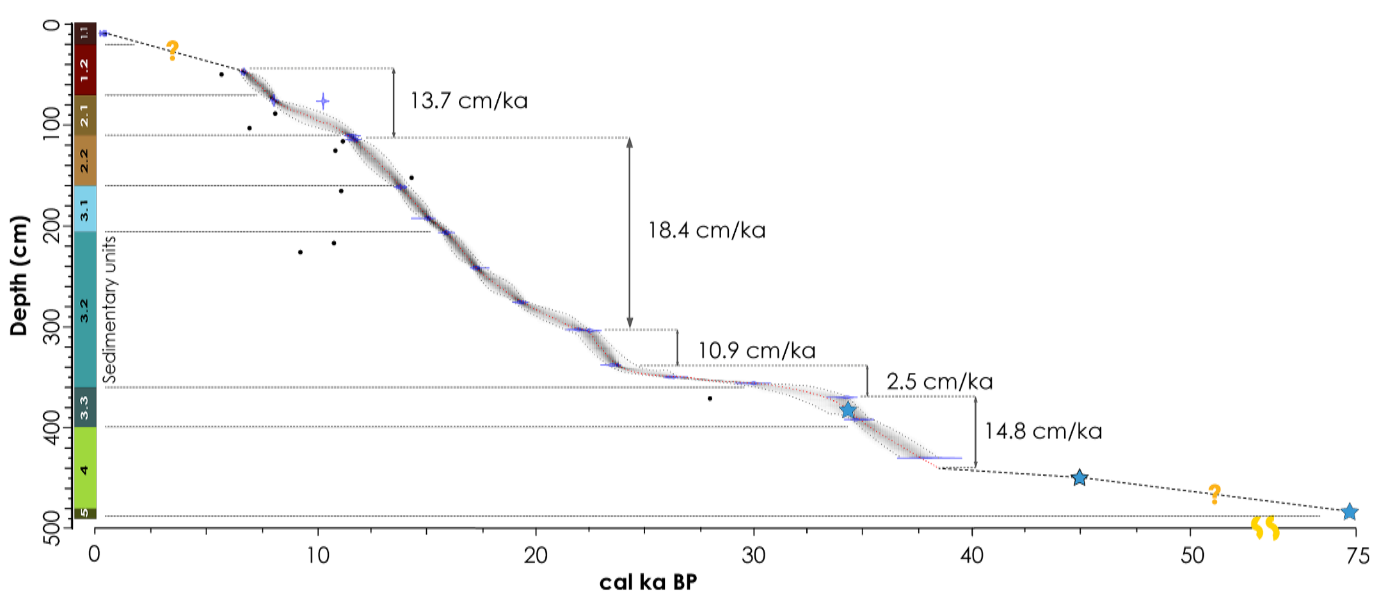

Fig. 3. Chronological model of Pllan d'Están sedimentary sequence based on 19 AMS dates with their uncertainty (dark blue) and 3 OSL (blue stars) dates. Sedimentation rates are indicated as cm per ka. Coloured bar indicates the Sedimentary Units, and the horizontal black lines its limits. Question marks indicate possible hiatus in the sequence. Black dots indicated the discarded dates. (For interpretation of the references to colour in this figure legend, the reader is referred to the web version of this article.)

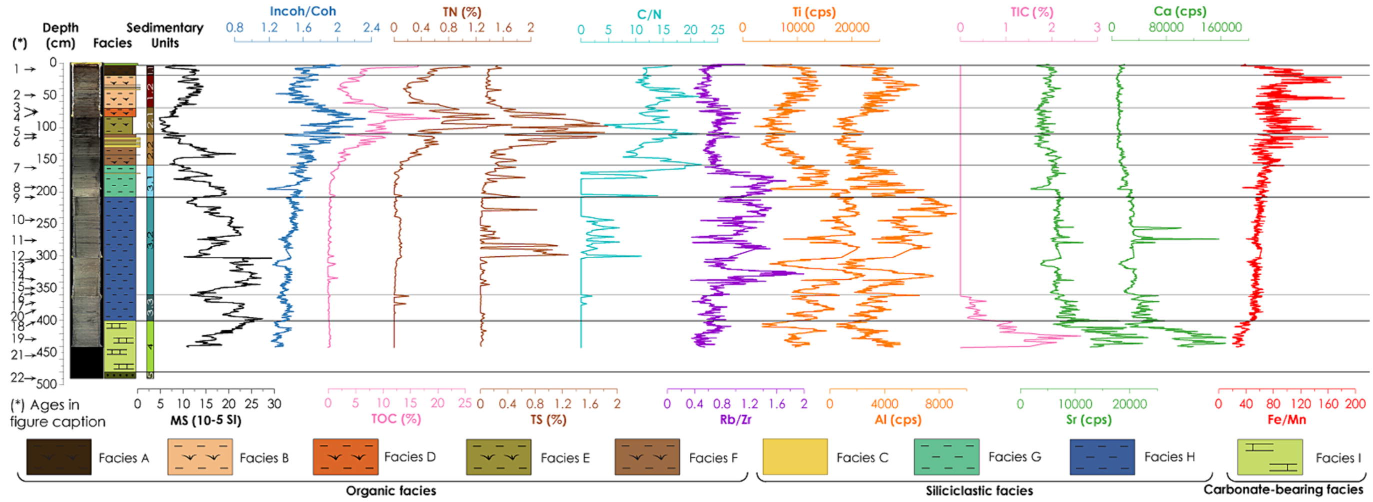

Fig. 4. Sedimentary facies and units. Magnetic susceptibility (MS), Incoh/Coh ratio, percentage of total organic carbon (TOC), total nitrogen (TN), total sulphur (TS), C/N and Rb/Zr ratios, the main XRF data associated with siliciclastic inputs (Ti, Al), total inorganic carbon (TIC), other XRF data (Sr and Ca) and Fe/Mn ratio. XRF of all the elements analysed area shown at the repository data. Black horizontal lines correspond to units' limits. The number of the dates are referred to the ID field of Table 1 and correspond with: 1: 0.18 cal ka BP; 2: 6.6 cal ka BP; 3: 8.0 cal ka BP; 4: 10.2 cal ka BP; 5: 11.4 cal ka BP; 6:11.7 cal ka BP; 7: 13.8 cal ka BP; 8: 15.0 cal ka BP; 9: 15.9 cal ka BP; 10: 17.2 cal ka BP; 11: 19.3 cal ka BP; 12: 21.9 cal ka BP; 13: 22.6 cal ka BP; 14: 23.6 cal ka BP; 15: 26.2 cal ka BP; 16: 29.8 cal ka BP; 17: 34.2 cal ka BP; 18: 34.8 cal ka BP; 19: 38.2 cal ka BP; 20: 34.7 cal ka; 21: 46.7 ka; 22: 74.9 ka.

groups, according to their association to main mineral phases along the master sequence (Fig. 4) and the correlation analyses (Table S1 in *Supplementary Material*): (1) siliciclastic (Al, Si, Mn, K, Ti and Fe); (2) carbonatic (Ca, Sr, well correlated with TIC values); (3) Pb and Zn, with no correlation with any other variable, and likely related to atmospheric deposition. The siliciclastic-related elements have higher values in the lower section (450–170) with several peaks and a general increasing trend upwards. The Rb/Zr ratio is considered an indicator of grain size in marine and lacustrine silty sediments (Wu et al., 2020) since Rb is likely more abundant in clay minerals (finer fraction) and Zr in heavy minerals (coarser fraction). The Rb/Sr has low values in the carbonate/bearing basal section, and progressively increased in the siliciclastic sediments (up to 170 cm) with four large fluctuations marking alternating intervals of dominant coarser and finer sedimentation. The organic rich sediments of the upper 170 cm have lower Rb/Zr ratios suggestive of less clay content associated to dominant runoff instead of finer glacial sediments. MS profiles are generally inverse to Rb/Zr as most magnetic particles are in the coarser fractions. Higher siliciclastic content is associated to higher clays and quartz percentage as observed in the smear slides. Ca and Sr values are low in most of the sequence and only reach higher values at the base and some peaks around 250–300 cm. TIC and Ca values are highly correlated, so Ca can be used as an indicator of calcite content (Moreno et al., 2011). Finally, Incoh/Coh ratio, according to its association to the presence of organic matter, reaches the maximum values at the top of the sequence. Incoh/coh ratio varies parallel to TOC content, thus could be used an excellent high-resolution indicator of organic matter accumulation (Chawchai et al., 2016). The Fe/Mn ratio has been used as a redox condition indicator (Kwiecien et al., 2014). The profile has low values (more oxidizing conditions) in the lower sections (450–160 cm) and higher but variable in the upper 160 cm.

In order to objectively describe the variance of these large dataset, a PCA (Fig. 5) was carried out using 17 variables (TIC, TOC, TN, TS, Zn, Pb, Y, Al, Ti, Si, Pb, Fe, K, Mn, Zr, Sr, Ca) and 221 cases. The first two eigenvectors comprise the 73.42 % of the total variance (51.23 % correspond to eigenvector 1). Eigenvector 1 is controlled by TOC, TN and TS, at the negative end while all the other elements associated to siliciclastic input appear at the positive end. Thus, this eigenvector represents the variation among the organic and the siliciclastic content. The second eigenvector (22.20 % of variability) is controlled by TIC, Ca and Sr at the negative end and Pb and Zn at the positive end, thus

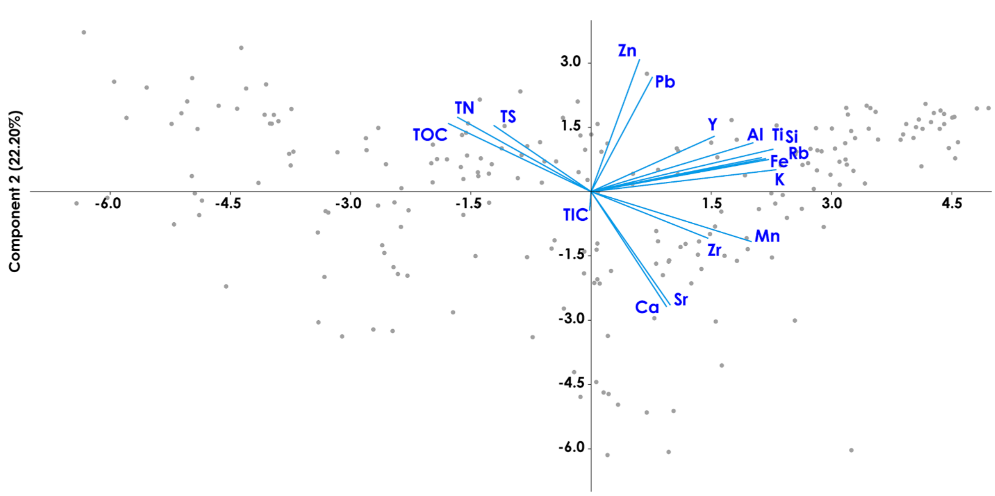

Fig. 5. Principal component analyses carried out with X-ray fluorescence data, and percentages of TOC, TIC, TN and TS from Pllan d'Están paleolake sequence.

representing the presence of carbonates in the sediment and the heavy metals associated to atmospheric deposition.

4.5. Sedimentary facies

Nine facies were identified considering visual description, microscopic observation of smear slides and geochemical composition. Sedimentary facies are classified into organic, siliciclastic and carbonate-bearing (Table S2, *Supplementary Material*).

(A) **Organic facies (>3.5 % TOC).** Five organic facies occur in the upper 160 cm of the composite sequence. They all have high TOC (mean > 3.5 %), TOC/TN values (10–20, Fig. 5), and high Fe/Mn and low Rb/Zr values. Facies A, B and F have a higher siliciclastic content while Facies D and E have the highest TOC content of the sequence. Organic matter is composed of plant remains of variable size and amorphous organic matter. They are interpreted as deposition in a peatbog-shallow lake environment with variable detrital input. More detrital facies represent periods with higher sediment input. Facies A are brownish, cm-thick banded, with abundant plants remains. Facies B is a grey, laminate, heterometric siliciclastic silt with diatoms and abundant amorphous organic matter. Facies F is composed of banded, organic-rich, silt and represent the transition from a lacustrine environment to a wetland-peatbog. Facies D (laminated) and E (banded) have the highest TOC values they represent deposition in a wetland – peatbog with restricted clastic input.

(B) **Siliciclastic facies.** Three siliciclastic facies have been identified (Fig. 5). They are characterised by almost no organic matter content, higher values of siliciclastic minerals and elements. Facies C occurs as intercalated mm-thick laminae in upper 35 to 172 cm. They are composed by brownish grey, fine sand, with some plant remains. They interpreted as deposition during intense flood events. Facies G occurs as light grey, mm-thick laminated, Q-Ft-rich silt. The darker laminae are coarser and contains more opaque minerals while light coloured laminae contain higher clay mineral content. Facies H are yellowish grey and brownish black, cm to mm-thick laminated, and composed of an alternation of (1) dark laminae with larger grains and plant remains (<10 %), (2) sandy mm-thick laminas with carbonates (<20 %), and (3) finer light laminae with more clay minerals (>10 %). Facies G and H represent deposition in a shallow lake fed by meltwaters of the nearby glacier.

(C) **Carbonate-bearing facies**. Facies I, the only carbonate-rich facies, is made of light grey and brownish black mm-thick, laminated siliciclastic silt with carbonates (TIC = 2 %). Light grey laminae are composed of finer, angular carbonate, quartz, feldspar and few biotite, clay minerals and opaque minerals while brownish black mm-thick laminae contain rounded larger size grains and more carbonates (Fig. 5).

4.6. Sedimentary units

According to sedimentary facies and geochemical data, 5 sedimentary units (hereafter Units) have been identified in the composite master sequence (Fig. 5):

Basal Unit 5 (490 to 480 cm). It is composed of coarse sand sediments with abundant granite clasts, likely corresponding to the basal till.

Unit 4 (480–400 cm), composed of Facies I and characterized by the occurrence of carbonate with the highest TIC (0.5–3 %), Sr (5000–25,000 cps) and Ca (30,000–170,000 cps) values of the sequence and the lowest organic content, Fe/Mn and Incoh/coh ratios. TIC and MS values decrease towards the top of this unit. Low Rb/Zr values are indicative of relatively coarse grain size of this Unit.

Unit 3 (400–160 cm) is composed by laminated siliciclastic Facies H and G. TOC values are near zero. Fe/Mn and Incoh/Coh ratios remain stable with a slight increasing trend to the top. Rb/Zr, Ti and Al present large ranges (0.4–2, 2000–20,000 cps and 500–10,000 cps, respectively) but with an increase trend towards the top. There are three main subunits:

- Subunit 3.3 (400–361 cm) is characterised by decreasing MS values (28–8 $\times$ 10^{-5}SI), presence of carbonates (TIC, 0.2–0.5 %) and decreasing values of Sr (5000–10,000 cps) and Ca (10,000–40,000 cps).
- Subunit 3.2 (361–208 cm) has oscillating MS values (lower in the laminated zones and higher in the more massive sections) and low Ca and Sr values (10,000 and 5000 cps, respectively). Rb/Zr profile shows three main peaks associated to finer grain in the laminated facies. The better laminated section (300–208 cm) present some C/N and TN and TS peaks suggestive of higher organic matter accumulation.
- Subunit 3.1 (208–160 cm) is composed of banded to laminated facies G, with the highest values of Rb/Zr (1–1.6) but lower values of other silicate/related elements (Al, Ti). A slight increase in organic matter is observed at the top of this subunit.

Unit 2 (160–70 cm) groups the most organic interval of the sequence.

- Subunit 2.2 (160–110 cm) groups Facies C, F and G, and it is characterized by increasing Incoh/Coh, TOC and TN values, decreasing MS, Ti and Al and lower Rb/Zr. The base of the unit is marked by a sharp decrease in Rb/Zr (~0.5) and a progressive increase of Fe/Mn (60–160).
- Subunit 2.1 (110–70 cm) has the sediment facies with the minimum values of MS (5-10x10^{-5}SI), and the highest organic matter content. The siliciclastic elements increase towards the top, Rb/Zr slightly increased and Fe/Mn decrease. TOC/N is above 12, but with one interval of lower values indicative of higher lacustrine organic matter input.

Unit 1 (70–4 cm) group organic facies A and B.

- Subunit 1.2 (70–20 cm) is characterised by lower Incoh/Coh, TN, TOC values and an increase in siliciclastic component while Fe/Mn ratio reaches the maximum values at the base and the top of the unit.
- -Subunit 1.1 (20–4 cm) is characterized by an increase of Incoh/Coh, TOC, TN, TOC/N and lower content of the siliciclastic elements, Fe/Mn, and higher Rb/Zr.

4.7. Palynology

The bottom sample of the master sequence was sterile, so the pollen stratigraphy started at the bottom of Unit 3, at 370 cm depth (Fig. 6), and defined 6 Pollen Zones (P.Z.1-P.Z.6).

- P.Z.6 (370–268 cm): This zone is characterized by the lowest values of arboreal pollen (AP) of the whole sequence. Trees and shrubs are dominated by *Pinus* and *Juniperus* including the maximum percentages of both *Ephedra* and Ericaceae and the presence of *Betula*. The highest values of *Artemisia* in Pllan d'Están occurred at the base of this zone (Fig. 6), as well as the maximum of the general herbaceous component (NAP). The percentages of aquatics (HH) increased, with the appearance and first development of *Ranunculus* at the top of this zone.
- P.Z.5 (268–208 cm): Pollen spectra was characterized by low taxa variety and poor pollen preservation. Pine dominated, coherent with its well-known over-representation in open vegetation areas. Isolated presence of similar taxa than in the previous zone (*Juniperus, Betula*, Ericaceae, *Ephedra*) and lower values of both NAP and HH groups

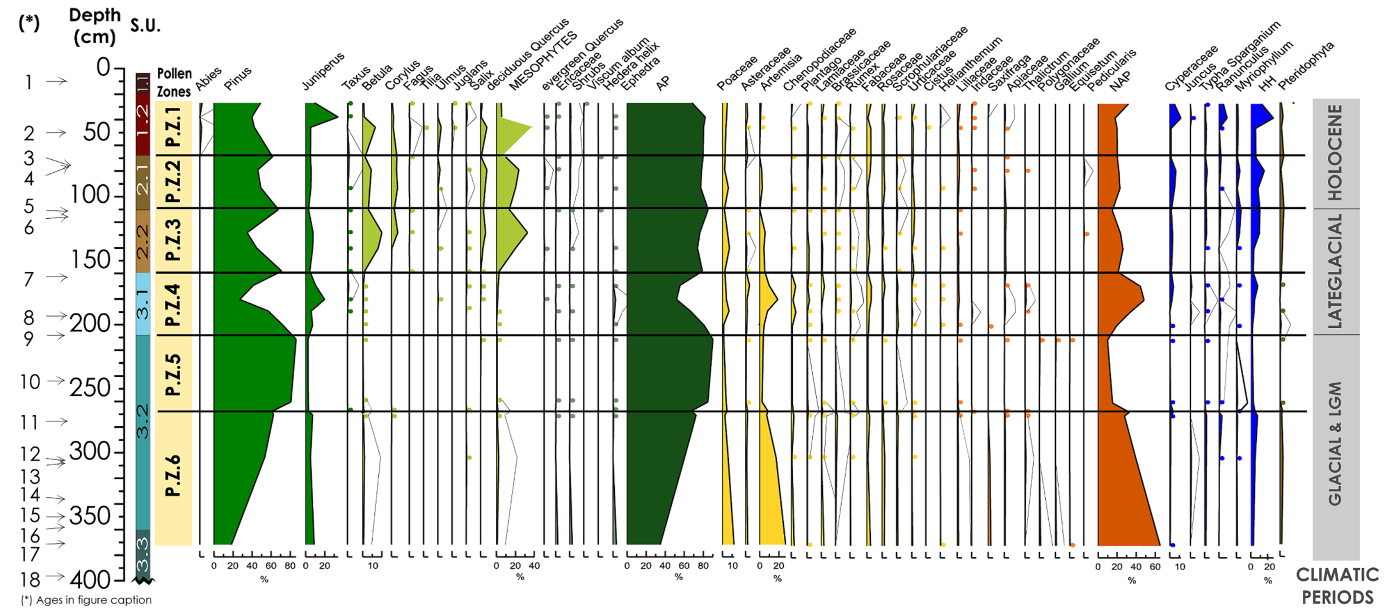

Fig. 6. Pollen diagram of Pllan d'Están lacustrine record with selected taxa. Mesophytes group is composed by *Betula, Corylus, Alnus, Fagus, Tilia, Ulmus, Juglans, Salix* and deciduous *Quercus*; and Pteridophyta by Monolete and Trilete indetermina spores as well as *Asplenium, Selaginella, Pteris, Anthyrium, Dryopteris* and *Cryptogramma crispa*. AP curve includes all the trees, shrubs and liana, NAP records the herbaceous component while HH is the result of the whole hygro- and hydrophytes (thus, aquatics including surrounding flooded lacustrine areas). Note that besides pollen zones from P.Z.6 at the base and P.Z.1 at the top, sedimentary units and sub-units are also indicated on the left, as well as radiocarbon dates located in depth. Main climatic periods boundaries are also included on the right part of the figure. Complete pollen diagram of Pllan d'Están lacustrine record are shown in the Fig. S2 of the *Supplementary Material* and at the repository data. The numbers of the dates are referred to the ID field of Table 1 and correspond with: 1:0.18 cal ka BP; 2: 6.6 cal ka BP; 3: 8.0 cal ka BP; 4: 10.2 cal ka BP; 5: 11.4 cal ka BP; 6:11.7 cal ka BP; 7: 13.8 cal ka BP; 8: 15.0 cal ka BP; 9: 15.9 cal ka BP; 10: 17.2 cal ka BP; 11: 19.3 cal ka BP; 12: 21.9 cal ka BP; 13: 22.6 cal ka BP; 14: 23.6 cal ka BP; 15: 26.2 cal ka BP; 16: 29.8 cal ka BP; 17: 34.2 cal ka BP; 18: 34.8 cal ka BP.

completed the typical spectra corresponding to intensively glaciated areas.

- P.Z.4 (208–160 cm): This zone is characterized by the development of pioneer *Juniperus* and the decreasing values of *Pinus* (Fig. 6). *Artemisia* dominated among the herbs but after this zone, its values decreased progressively until almost disappearing in the upper part of the sequence as well as other typical taxa of Glacial/Lateglacial spectra such as *Ephedra,* Chenopodiaceae, Cichorioideae, *Plantago*, Lamiaceae or *Rumex,* among others (*Supplementary Material* Fig. S2). Cyperaceae started its development and a higher variety of hydrophyte taxa was recorded with fluctuating values.
- P.Z.3 (160–110 cm): During this zone, a clear change occurred both in percentages and taxa composition of arboreal pollen taxa. The rapid and large peak of *Betula* marked this zone, followed by the development of *Corylus* and deciduous *Quercus*. *Pinus* fluctuated and *Juniperus* maintained similar values than in P.Z. 6. *Fagus* appeared for the first time and it was present, although reduced, till the top of the sequence. Poaceae and *Artemisia* co-leaded the herbaceous formations, and *Myriophyllum*, typical aquatic taxa, reached its maximum percentages of the sequence (Fig. 6).
- P.Z.2 (110–70 cm): This zone contained some *Pinus* fluctuations while *Juniperus* and *Betula* decreased. The NAP component maintains similar values despite an important decrease of *Artemisia*. Aquatics, increased again with fluctuations, led by Cyperaceae and *Myriophyllum*.
- P.Z.1 (70–30 cm): The upper palynological zone is noticeable by the presence of both *Abies* and *Tilia* (Fig. 6). The AP percentages were still high, with *Pinus* and *Juniperus* showing a co-leading role with opposite trends. So, conifers dominated but the main taxa fluctuated. The herbaceous component was varied and not too relevant while a significant increase of HH occurred at the top of this zone, due to a peak in both Cyperaceae in the hygrophytes group and *Ranunculus* as hydrophytes, pointing fluctuating water levels.

4.8. Diatoms stratigraphy

Diatoms were absent in the lower sections of the sequence. A total of 24 samples of diatoms have been analysed covering the uppermost 225 cm to assess changes in lake environmental conditions. The results showed four main diatoms zones (Fig. 7). However, due to the low resolution, the boundaries of each zone are approximate.

In the lower zone (D.Z.4; 225–190 cm), a unique diatom assemblage of benthic diatom species had the highest abundance (relative) across the entire record: *Amphora* cf. *eximia* (50 %), *Gyrosigma acuminatum* (48 %), *Caloneis fontinalis* (10 %) and *Nupela gracillima* (10 %). These diatoms have lower abundance than the more recent diatoms assemblages analysed. PCA component 2, which explains the 19.6 % of diatom variability, summarised the diatom changes in this zone.

In the next zone (D.Z.3; 190–150 cm) a new assemblage appeared, where *Achnanthidium minutissimum* sl. (60 %) and *Gomphonema* cf. *minusculum* (22 %), *Gomphonema lateripunctatum* (18 %), were the dominant diatom species. These diatoms are also abundant in the most recent Pllan d'Están diatom sample analysed.

The next zone (D.Z.2; 150–35 cm), was the longest zone in record. It was characterised by a dominance of small fragilaroids taxa such as *Stuarosira venter* (25–35 %), *Staurosira* spp. (10–25 %) and *Pseudostaurosira* spp. (10–40 %) and *G. lateripunctatum* (22 %). This zone could be divided into two subzones. In addition, this subzone was characterised by the occurrence of the planktonic diatoms *Pantocsekiella* spp. In the lower subzone (D.Z.2B 150–105 cm) a large increase (>25 %) in *Amphora pediculus* was observed. PCA component 1, which explains the 34 % of diatom variability, summarised the changes in species assemblages of this zone..An increase in *A. minutissimum* sl., *G. lateripunctatum, Denticula tenuis* and *Nitzschia denticulata* parallels a decrease on *Pseudostaurosira* spp., characterised the upper subzone (D.Z.2A 105–35 cm).

Finally, the upper zone (D.Z.1; 4–35 cm) showed a significant change in species abundance. *A. minutissimum* sl. increased considerably became the dominant species in the diatom assemblage. This increase paralleled

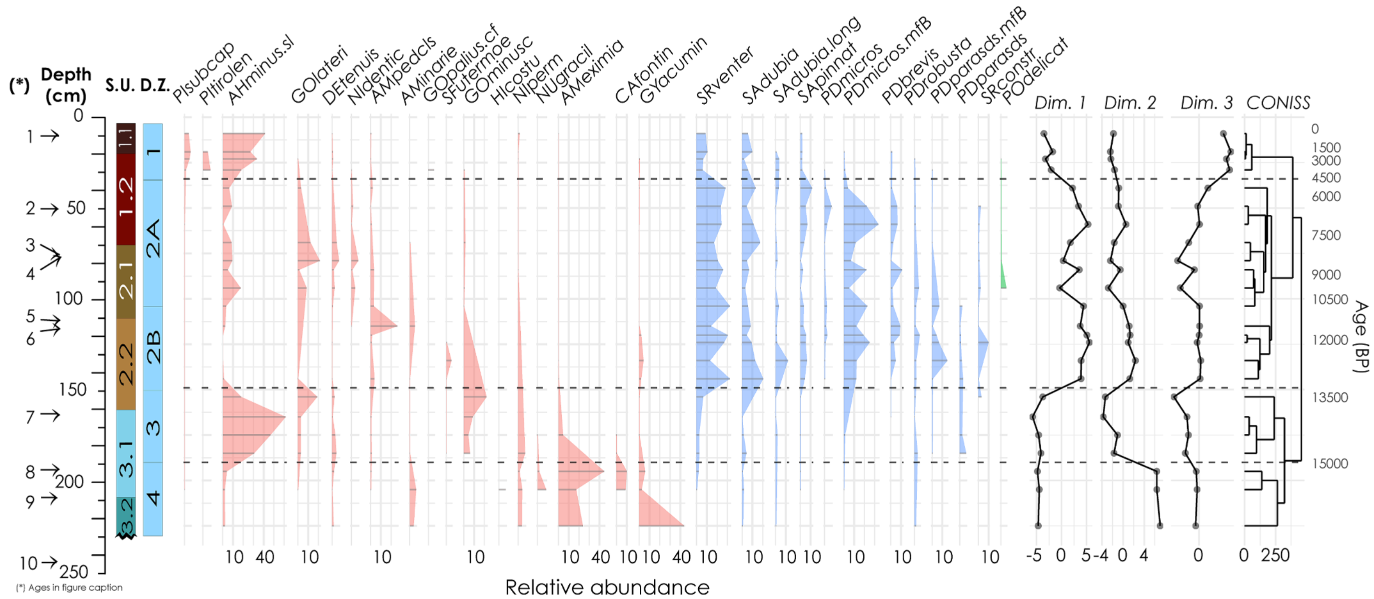

Fig. 7. Diatoms diagram of Pllan d'Están lacustrine record with selected taxa. Plots referred as "Dim." show the variation of the three main components of the PCA through depth. Note that besides diatoms zones from D.Z.4 at the base and D.Z.1 at the top, sedimentary units and sub-units are also indicated on the left, as well as radiocarbon dates located in depth. Red plots corresponds to benthonic diatoms, blue to tychoplanktonic diatoms and green to planktonic diatoms.The number of the dates are referred to the ID field of Table 1 and correspond with: 1:0.18 cal ka BP; 2: 6.6 cal ka BP; 3: 8.0 cal ka BP; 4: 10.2 cal ka BP; 5: 11.4 cal ka BP; 6:11.7 cal ka BP; 7: 13.8 cal ka BP; 8: 15.0 cal ka BP; 9: 15.9 cal ka BP; 10: 17.2 cal ka BP. The code of diatoms are referred to: AHminus.sl: *Achnathidium minutissimum* sl.; AMinarie: *Amphora* cf. *Inariensis*; AMeximia: *Amphora eximia*; AMpedcls: *Amphora pediculus*; CAfontin: *Caloneis fonticola*; DEtenuis*: Denticula tenuis*; GOlateri: *Gomphonema lateripunctatum*; GOminusc: *Gomphonema minusculum*; GOpalius.cf: *Gomphonema parvulius*; GYacumin: *Gyrosigma accuminatum*; HIcostu: *Hippodonta costulata*; NIdentic: *Nitzschia denticulata*; NIperm: *Nitzschia perminuta*; NUgracil: *Nupela gracillima*; POdelicat: *Pantocsekiella delicatula*; PIsubcap: *PInnularia subcapitata*; PItirolen: *Pinnularia tirolensis*; PDmicros: *Psedostaurosira microestriata*; PDrobusta: *Psedostaurosira robusta*; PDparasds.mfB: *Pseudoestaurosira* cf. *Parasitoides*; PDbrevis: *Pseudosstaurosira brevistriata*; PDmicros.mfB: *Pseudosstaurosira microestriata mf B*; PDparasds: *Pseudostaurosira parasitoides*; SFutermoe: *Sellaphora utermoehlii*; SRconstr: *Staurosira construens*; SRventer: *Staurosira venter*; SAdubia: *Staurosirella dubia*; SAdubia.long: *Staurosirella dubia mf A*; SApinnat: *Staurosirella pinnata*; (For interpretation of the references to colour in this figure legend, the reader is referred to the web version of this article.)

a large decrease in small fragilaroid taxa (*Pseudostaurosira* spp., *Staurosira venter* and *Staurosirella* spp.). However, the occurrence of *Pinnularia* spp. such as *Pinnularia subcapitata*, *Pinnularia* cf. *tirolensis*, *Pinnularia subrupestris*, *Pinnularia krammeri* and the arophilic *Pinnularia borealis* were a unique feature of this zone in the entire diatom record. A large change excursion in PCA axis 3, which explains the 10.6 % of diatoms variability characterised this zone.

5. Climate variability and landscape evolution in the Ésera valley based on Pllan d'Están paleolake sequence

This multiproxy study of Pllan d'Están paleolake sediments allows reconstructing glacial evolution phases in the Ésera valley during the last glacial cycle, in combination with past climate evolution and vegetation history at a local and regional scale. We have identified six main phases since the maximum glacier extent.

5.1. Maximum glacier extent (prior to 74.9 ka BP; 490–480 cm depth). Unit 5

The glacial till with sandy matrix and granite and limestone pebbles at the base of the sequence was dated by OSL at 74.9 ka BP. The occurrence of this till suggests the presence of basal moraine at the Pllan d'Están basin deposited by the Ésera glacier during its maximum advance (PLGM ca. 60 ka BP; Lewis et al., 2009). The thickness of till deposits in the basin is unknown and it could span several glacial cycles. It is also likely that some till was eroded by the retreating glacier, so the sequence is not complete and its sedimentary continuity cannot be guaranteed at the top of Unit 5 (Fig. 5). The glacier during extreme cold conditions would have been characterized by very cold ice and a low amount of subglacial flux thus leading to a minor supply of sediments by the expected reduced water discharges (Greenwood and Hughes, 2022; Patton et al., 2022).

5.2. The onset of the lacustrine sedimentation (ca. 46.7–34.8 ka BP; 480–395 cm depth). Unit 4

This period represents the development of a lake in the over-excavated and till-covered Pllan d'Están basin. During this stage, rhythmic, laminated, carbonate-rich lacustrine deposits started to fill the basin. The presence of carbonate sediments in the sequence (Figs. 5 and 8) is associated with runoff from the catchment area since the observed calcite particles (irregular, heterometric, without euhedral faces) do not have the features of authigenic carbonates resulting from changes in lake water chemistry. The occurrence of carbonate-bearing grains in the subglacial-proglacial sediments indicates that a source area with ice-free carbonate formations was exposed when the glacier retreated up to the Pllan d'Están basin. Most likely, the source area was the lake basin itself, mostly dominated by limestone (Fig. 1), specially around the lake and up to 2 km upstream of the Ésera valley. Other examples of lacustrine rhythmites with carbonate content in silicate areas have been described in Tramacastilla Lake (western central Pyrenees, García-Ruiz et al., 2003) and Sant Maurici Lake (eastern Pyrenees; Calero et al., 2016). In Tramascastilla, changes in the surface drainage during deglaciation caused by a landslide blocked the lake basin from upstream carbonate-rich formation. In Sant Maurici, the retreat of the glacier, exposed carbonate rock formations that were the main supply of sediments to the lake for a short period; as glacier retreated further the contribution of the granite watershed was dominant. However, the occurrence of carbonate formations in the watershed is not enough to secure carbonate deposition in lakes during glacial times. Several examples show that temperature may be a determinant

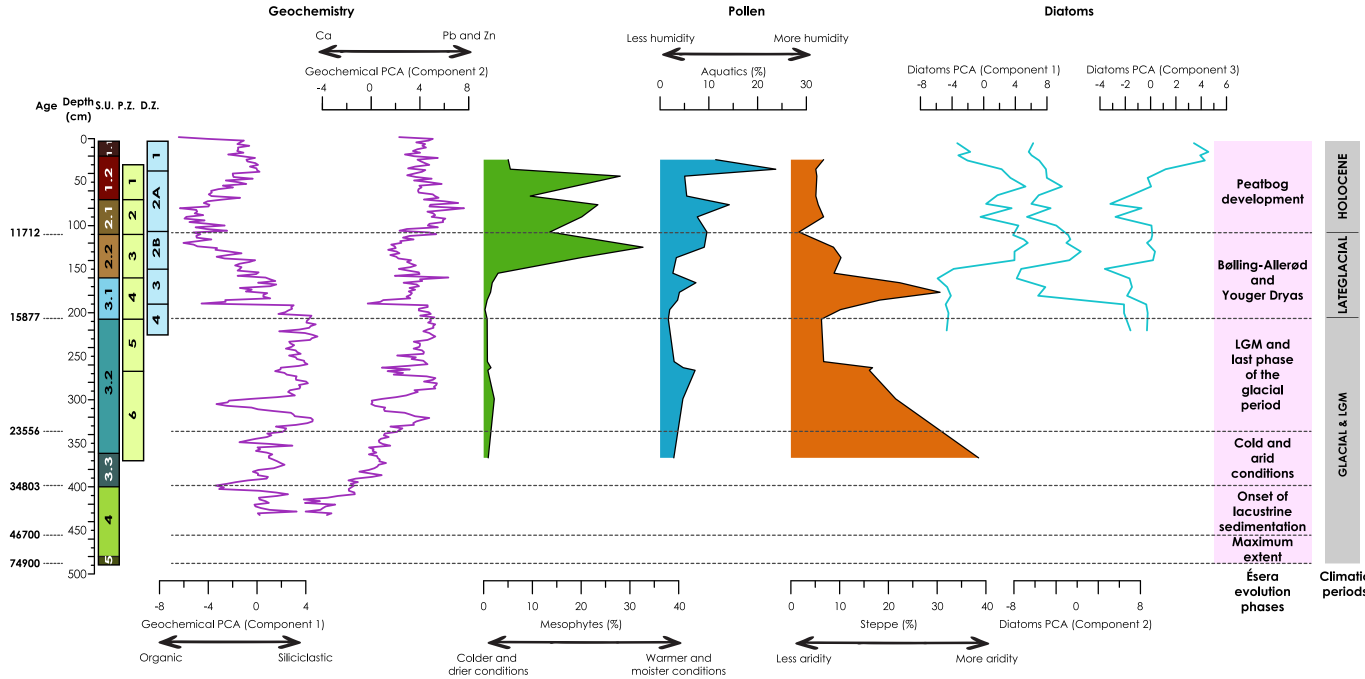

Fig. 8. Main geochemical, palynological and diatoms characteristics of Pllan d'Están sequence. Purple graphs correspond to the geochemical PCA, component 1 distinguished between organic and siliciclastic content, and component 2 between Ca and the combination of Pb and Zn content. The three groups of pollen taxa (green, blue and orange graphs) are: Mesophytes (*Betula, Corylus, Alnus, Fagus, Tilia, Ulmus, Juglans, Salix,* decidous *Quercus*), Aquatics (Cyperaceae, *Juncus, Typha-Sparganium, Ranunculus*, *Myriophyllum*) and Steppe (*Myrica, Ephedra fragilis* type*, Ephedra dystachia* type, Cichorioideae, Asteroideae, Carduae, *Centaurea, Artemisia*, Chenopodiaceae, Caryophyllaceae, *Plantago,* Brassicaceae, *Rumex, Helianthemum*). Three blue graphs are diatom variability's three main components (PCA). Environmental interpretation and chronological phases are also indicated. (For interpretation of the references to colour in this figure legend, the reader is referred to the web version of this article).

factor, as carbonatic particles dissolved more rapidly in cold waters. In Enol Lake, a lake located in a carbonate-dominated area of the Cantabrian Mountains, the presence of carbonates in the sediment during glacial times was associated to warmer climates when not so cold waters were unable to totally dissolve the carbonates arriving by runoff to the lake (eg. ca. 37 ka BP and during the Holocene; Moreno et al., 2010). A similar situation is observed in Marboré Lake sediments (Cinca valley, Central Pyrenees; Oliva-Urcía et al., 2018), where in spite the lake is surrounded by limestones, carbonates are rarely found in the sediments of the last 14 ka BP except during slightly warmer periods.

In Pllan d'Están, the glacier was likely very close to the lake basin during this period and thus the higher areas of the valley that are dominated by granites were still fully covered by ice. In such a situation, the erosion of limestones in the surroundings of the lake (see Fig. 1c) by melting waters and small creeks would preferentially supply carbonates by runoff to the lake compared to less siliciclastic material arriving from the erosion of granites and shales totally covered by the glacier. Probably, the presence of carbonates in Pllan d'Están requires also higher temperatures to ensure carbonates would not be completely dissolved. Higher sedimentation rates during this period, particularly from 38.4 to 34.8 cal ka BP, is also coherent with relatively warmer climates associated to some intervals within the MIS 3 compared to the colder LGM (González-Sampériz et al., 2020). Once the glacier retreated further up in the valley, the area available to be eroded was much larger than during this short period and siliciclastic sources predominated over the local limestone (Fig. 1b), thus progressively minimizing the presence of carbonate in the sediments during the remaining sequence.

During this stage covering from 46.7 ka BP to 34.8 ka BP, the sediments were barren of diatoms or pollen grains (Fig. 8) indicative of very limited biological productivity in the lake and a regional landscape devoid of vegetation. The relatively low Rb/Zr ratio is coherent with relatively coarser grain size of this facies, and the low Fe/Mn values, with deposition in a shallow lake with high oxidation rates. These cold, arid conditions are in coherence with other regional records spanning the MIS 3, as La Larri (Central Pyrenees; Salazar-Rincón et al., 2013), or El Cañizar de Villarquemado (Iberian Range; González-Sampériz et al., 2020).

5.3. *Cold and arid conditions in a glaciated landscape (34.8–23 ka BP; 393–338 cm depth). Unit 3, P.Z.6*

The carbonate content decreased rapidly, although still the silt at the base of Unit 3.3 had some carbonate grains (TIC < 0.5 %). The first lacustrine sediments with no carbonate grains could have been deposited in a subglacial lake, as the ice tongue still covered the basin and sediment input was through the base of the glacier, with sources in the granite watershed. Subglacial and proglacial sediments are not easily differentiated in the sedimentary sequences (Livingstone et al., 2022,2015,2012). Rhythmites (Facies H, Fig. 5) were made of siliciclastic banded to laminated silts (high values of Ti, Al, positive values in geochemical PCA-1 component in Fig. 3) indicating that siliciclastic rocks (shales, granite, etc.,) were dominant (over limestones) in supplying sediment to the lake. The rhythmic nature of lamination is marked by different grain-size of the particles indicating a glacier environment marked by strong seasonality and extremes of temperatures (Leonard and Reasoner, 1999; Ohlendorf et al., 2003): the coarse, angular silt laminae deposit corresponding to the melting season and the fine silt laminae to the ice-covered season when fine particles settled by suspension. The rhythmic nature of the lamination points to changes in the sediment and water input caused by seasonal melt waters dynamics.

The very low sedimentation rate at this period indicates a low supply of sediments by runoff and likely cold and arid conditions in a catchment area that was mostly ice-covered during this period. Palynological results support cold and arid conditions, consistent with the scenario described by other global and regional sequences such as El Portalet (González-Sampériz et al., 2006) or El Cañizar de Villarquemado

(González-Sampériz et al., 2020) for this time period. At the beginning of P.Z.6 the herbaceous component dominated with the highest NAP values of the whole sequence, being *Artemisia* the predominant taxa next to Poaceae and other steppe taxa such as Chenopodiaceae, Asteraceae or both *Ephedra dystachia* and *E. fragilis* types (Figs. 6 and 8, Fig. S2 in the *Supplementary material* and *repository data*). The tree component included relatively low percentages of conifers (*Pinus* and *Juniperus*) and the isolated presence of *Betula, Salix* and *Myrica* (see complete diagram Fig. S2 in the *Supplementary material* and *repository data*), as well as Ericaceae. This same distribution pattern is recognized in the previously mentioned El Portalet palynological sequence, located in a similar altitude also in the Central Pyrenees, but in a western location (González-Sampériz et al., 2006).

5.4. The global last glacial maximum and last phase of the glacial period (23–15.9 ka BP; 338–207 cm depth). Unit 3, P.Z.6 and P.Z.5

In Pllan d'Están sequence, the global LGM is identified by an increase in the sedimentation rate, higher values of MS and a sharp decrease in Rb/Zr and geochemical PC1 all indicative of coarser sedimentation, but there was no significant identification in pollen assemblages. In fact, pollen spectra are characterized by low taxa variety and poor pollen preservation. Dominance of pollen pines is relevant but coherent with its well-known over-representation in open vegetation areas. Isolated pollen grains of similar taxa than in the previous phase (*Juniperus, Betula*, Ericaceae, *Ephedra*) and lower values of both NAP and HH groups complete the typical pollen spectra corresponding to intensively glaciated areas. The recorded sedimentological features are not coherent with a glacier readvance during this period. We cannot rule out that erosion in the glacier bed increased during the LGM, due to an increase in the ice thickness and in the velocity of ice displacement, although there is no evidence. However, in El Portalet, a clear sedimentological and palynological hiatus was identified and interpreted as a glacier readvance between 22.5 and 18 cal ka BP. In fact, cold but arid conditions attributed to this period in the Pyrenees, as well as in northeastern Iberia, prevented a regional maximum glacier advance (Bartolomé et al., 2021; González-Sampériz et al., 2020, 2017; Sancho et al., 2018).

Deposition after the global LGM was marked by a decrease in MS values and small changes in the sediment composition: siliciclastic silts were still mostly barren of organic matter, but TN increased and TOC/TN (<12) during a short interval ca. 19–17 ka BP pointed to some algal production in the lake.

After the LGM, in Pllan d'Están still poor variety and poor preservation of palynological taxa support the colder and more arid conditions previously shown in other marine and terrestrial records during Heinrich event 1 (Cacho et al., 1999; González-Sampériz et al., 2017, 2006; Jalut et al., 1992; Morellón et al., 2008; Reille and Lowe, 1993), as well as in nearby regional sequences such as Estanya lake by a decrease in the diatom productivity (Morellon et al., 2009), high values of *Artemisia* and steppe herbs, and fluctuating pollen sterility levels because of aerial exposure episodes (González-Sampériz et al., 2017). The development of *Ranunculus* started at the top of P.Z.6 agrees with other regional Pyrenean sequences of high altitude, both in the northern and southern slopes (González-Sampériz et al., 2006; Jalut et al., 1992, 1982).

5.5. The Bølling-Allerød and the Youger Dryas: Climate differences with northern Europe (15.9–11.7 ka BP; 207–115 cm depth). Unit 3 and Unit 2, P.Z.4 and P.Z.3, D.Z.4, D.Z.3 and D.Z.2

The onset of the Bølling interval was characterized by deposition of facies G (Unit 3.1) with a slight increase in organic matter while siliciclastic component was reduced (lower Al, Ti, more negative values in the geochemical PCA Component 1, Fig. 8) and finer grain size (the highest Rb/Zr ratio). Fe/Mn ratio continued the increasing trend from previous stage suggesting an increase in the depth of the water column and more anoxic conditions. The pollen taxa (P.Z.4), suggest a slight increase of temperatures, despite still prevailing arid conditions. *Juniperus* peaked during this period, as it happened at a regional scale during the Lateglacial because of its pioneer character (González-Sampériz et al., 2017), while NAP dominated led by *Artemisia* together with steppe herbs and shrubs and indicators of open vegetation formations (Chenopodiaceae, *Plantago*, again *Ephedra*, Fabaceae, Lamiaceae, etc.) (see complete diagram Fig. S2 in the *Supplementary data* and in the *repository data*). The same *Artemisia* expansion shown in Pllan d'Están during this interval is recorded regionally on Spanish and French palynological sequences of the Pyrenees, peaking around 14 ka cal BP too (González-Sampériz et al., 2017, 2006; Jalut et al., 1992; Montserrat Marti, 1992; Reille and Lowe, 1993). After the *Artemisia* peak, a rapid decreasing trend till the end of the Lateglacial paralleled a general humidity and temperature increase.

The Bølling period corresponds roughly to D.Z.3 and D.Z.4. The presence of *Stephanodiscus* (planktonic diatom) reinforces the scenario of higher lake level. The dominance of *Gyrosigma accuminatum* and *Amphora eximia* indicates higher trophic conditions consistent with anoxic conditions. The dominance of the pioneering and cosmopolite diatoms *A. minutissimum* sl., the abundance of *Gomphonem*a spp. and decrease of the diatoms that characterized the previous lake state (D.Z.4) indicates a richer lake environment, in terms of nutrient availability and diatom biodiversity.

The Allerød interval (GI-1a; 13.8–11.7 ka cal BP), was characterized by warmer and moister climate conditions clearly marked by the transition to Unit 2 with increasing organic matter deposition and a significant increase of both AP general values and taxonomic diversity in P.Z.3, probably associated to an enhancement of local pollen productivity. A significant decrease in *Pinus* percentages is recorded in relation to the nearby development of, first *Betula* and then *Corylus* and deciduous *Quercus,* showing the usual pattern and succession of mesophytes during this period both in the Pyrenees and main European sequences (Fletcher et al., 2010; González-Sampériz et al., 2017). Moister conditions can also be deduced by low values or even disappearance of steppe taxa as well as the development of aquatic taxa associated to changing environments, and also, by the presence of planktonic diatoms (Fig. 7). Particularly noticeable are the values of *Myriophyllum* in the upper part of P.Z.3, which continued during the beginning of the Holocene pointing to higher water levels.

Interestingly, the pattern of improved climate conditions with warmer temperatures and more humidity developed along the GI-1 (Greenland Interstadial 1) or Bølling-Allerød period differs from the typical last deglaciation trend in other European records where the transition at the GI-1 onset is abrupt and the warmest climates were found at GI-1e (Bølling) with a decreasing temperature trend along GI-1. The same warming trend during GI-1 observed in our Pyrenean record was previously described in sea surface temperature reconstructions from Western Mediterranean marine sediment records (Cacho et al., 2001) and from western Mediterranean temperate forest development (Combourieu Nebout et al., 2009). Despite the compelling evidence, there is still no clear explanation for the causes of these different latitudinal patterns (Moreno et al., 2014).

The Younger Dryas is the last cold stadial phase before the beginning of the current interglacial (Rasmussen et al., 2014). This interval corresponds to the upper part of Unit 2.1 with deposition of facies F but it was characterized by the occurrence of numerous facies C associated to more frequent extreme flooding episodes in the basin. In other high-altitude Pyrenean lakes such as El Portalet or Marboré (González-Sampériz et al., 2006; Leunda et al., 2017), this cold, short period is not easily characterized. Due to the low time resolution of the sampling no palynologic response was identified even in Pllan d'Están. This period corresponds to the onset of the diatom assemblage D.Z.2B (ca, 13–11.7 ka BP) and points to a large change in environmental conditions around 13 ka BP. This zone is characterised by a large increase in small thycoplanktonic cold-tolerant fragilaroid and post-glacial pioneering taxa (Smol, 2011). These taxa are abundant in high-altitude alpine lakes

(Lotter et al., 1997) and polar lakes. The dominance of these taxa characterizes the late-glacial history of many lakes in Europe and North America (Lotter et al., 1995 and references therein). In Pllan d'Están sequence, the dominance of fragilaroid taxa could be related to an increase in cold-meltwater runoff from the glacier.

5.6. A peatbog development during the Holocene (11.7 ka BP – Present-day; 115–4 cm depth). Unit 2 and Unit 1, P.Z.2, D.Z.1

The onset of the Holocene is marked by deposition of organic rich facies E in a wetland environment, progressively more extensive than the shallow lake areas. Although most organic matter accumulated was likely of terrestrial and aquatic plants, the lower TOC/TN ratio during 11.7–11.4 cal ka BP point to dominance of the lacustrine productivity. The basin was mostly occupied by wetland environments and the fluvial influence was greatly diminished. The Ésera Glacier would have been retreated further up closer to the cirques.

The vegetation composition of Pllan d'Están area during the Early Holocene (P.Z.2) was a mixed forest characterized by fluctuating but relatively high percentages of *Pinus* and secondarily *Betula*, and similar proportions of both *Corylus* and *Quercus* compared to the Allerød. The forest would have contributed to the reduced sediment input to the basin. These spectra are relatively similar to those found in Basa de la Mora, Marboré, Portalet, Tramacastilla or Estanya Pyrenean lakes, as well as in other northeastern sequences such as Villarquemado in the Iberian Range (González-Sampériz et al., 2020, 2017; Leunda et al., 2017; Pérez-Sanz et al., 2013). NAP values were low and steppe taxa mostly anecdotic. The first occurrence of *Tilia* at around 6.5 ka BP and the continuous development of *Abies* were coherent with its regional appearance, expansion and chronology (González-Sampériz et al., 2006; Leunda et al., 2017; Miras et al., 2007; Pérez-Sanz et al., 2013). Hygro-hydrophytes, however, maintained an increasing trend with a first large expansion of Cyperaceae during the early development of peatbog areas: the occurrence of adjacent lacustrine environments in the same basin is indicated byhigh percentages of *Myriophyllum*.

Diatoms assemblages during the early Holocene (D.Z.2A) where richer and showed a general tendency to a decrease in *Pseudostaurisira* spp. and an increase in *A. minutisima* sl., a dominant species in today's Pyrenean lakes diatoms assemblages. The Holocene associations are characterized by higher abundance of *Gomphonema* spp., *Denticula tenuis* and *Nitzschia denticulata* and lower occurrence of planktonic diatoms. The absence of mid to late Holocene sediments in the Pllan d'Están sequence suggests the erosion of the most recent sediment likely due to the distortion caused by the actual cattle grazing in this flat area. A similar pattern occurred in Sant Maurici lake (Easter Pyrenees), with a hiatus between ca. 8 and 4 cal ka BP (Calero et al., 2016). The Pllan d'Están wetland would have dried out during warmer and more arid phases in the Late Holocene (i.e., Holocene Thermal Optimum, 4 ka BP, Roman Period, Medieval Climatic Anomaly-MCA) and the upper sediment would have eroded. Sedimentation in the basin (Unit 1.1) restarted a few centuries ago, during the colder and relatively wetter phases of the Little Ice Age-LIA. At the top of the sequence (P.Z.1) conifers increased, mainly led by a large peak of *Juniperus*, suggesting drier conditions also shown by the sharp decrease of mesophytes and some peaks of shrubs, NAP, *Salix* or *Helianthemum,* probably related to open landscape expansion. Coherently, D.Z.1 was characterised by the abundance of *Pinnularia* spp. and some acidophilus and aerophilic taxa, indicating an established peatbog with lower water inputs from an inlet stream.

6. Conclusions

Pllan d'Están sedimentary sequence provided the longest lacustrine record of glacier, climate and environmental change in the Pyrenees with a robust chronology for the last 46.7 ka BP. Landscape evolution, limnological changes and vegetation history in the Ésera valley were reconstructed through a detailed multiproxy study that included sedimentological, geochemical and biological (pollen and diatoms) indicators, framed in a chronological framework based on ^{14}C and OSL dates. The basal till observed at the base of the Pllan d'Están record, and dated by OSL at 74.9 ka BP, represents the maximum extent of the Ésera glacier in the basin. At around 46.7 ka BP, lacustrine sedimentation starts in an environment where subglacial and proglacial phases probably alternate. First sediments recorded are composed by rhythmite carbonate-rich facies likely representing sedimentation during a warm stage in within MIS3 when carbonate grains supplied from nearby limestones was not totally dissolved. After this warmer period, cold and arid conditions dominated in a glaciated landscape (23–21 cal ka BP), as changes in facies composition, geochemical data and pollen taxa indicate. However, high sedimentation rates during this period, corresponding to the global LGM contradicts a hypothetical minor advance of the Ésera Glacier, as described in other Central Pyrenean valleys. The dominance of the herbaceous component despite pine's values (over-represented in an open landscape) and general poor pollen diversity and preservation implied that most of the catchment area was ice-covered until 15.9 cal ka BP.

The deglaciation of the valley started at 15.9 cal ka BP allowing to infer a different pattern from other European records. Thus, in the Ésera valley, as well as in other records of the Pyrenees, a trend to warmer and moister climate conditions define the Bølling-Allerød stage. Contrarily, most European paleoclimate records mark an abrupt transition at the onset of the Bølling period. The negligible glacial influence in the lake sediments, the increased bioproductivity and large changes in vegetation cover in the watershed, particularly the increase in mesophytes trees, characterize this period. The Younger Dryas (12.9–11.7 cal ka BP) was identified in the sequence by the dominance of cold-tolerant diatoms and the higher frequency of extreme flooding events in the basin. The onset of the Holocene is marked by the development of a peatbog environment, with regional vegetation characterized by a mixed forest including both conifers and mesophytes and an absence of steppe pollen taxa. Diatom assemblages at this time were very similar to today's Pyrenean lakes.

Pllan d'Están lacustrine sequence supports that maximum extent of Pyrenean glaciers occurred during MIS 4 instead of during the global LGM. Besides, a complex climatic period during last deglaciation with minor glacier advances and retreats has been described. This study stresses the asynchrony and differences of some climate changes with other regions of Europe at the end of last glacial period.

CRediT authorship contribution statement

Ixeia Vidaller: Conceptualization, Methodology, Formal Analysis, Investigation, Writing-Original Draft, Writing-Review & Editing, Visualization. **Ana Moreno:** Conceptualization, Methodology, Formal Analysis, Investigation, Writing-Original Draft, Writing-Review & Editing, Supervision, Project administration, Funding acquisition. **Penélope González-Sampériz:** Methodology, Formal Analysis, Investigation, Writing-Review & Editing. **Sergi Pla-Rabes:** Methodology, Formal Analysis, Investigation, Writing-Review & Editing. **Alicia Medialdea:** Methodology, Formal Analysis, Investigation, Writing-Review & Editing. **Miren del Val:** Methodology, Formal Analysis, Investigation, Writing-Review & Editing. **Juan Ignacio López-Moreno:** Conceptualization, Writing-Review & Editing, Project administration, Funding acquisition. **Blas Valero-Garcés:** Conceptualization, Writing-Review & Editing, Project administration, Funding acquisition.

Declaration of competing interest

The authors declare that they have no known competing financial interests or personal relationships that could have appeared to influence the work reported in this paper.

Data availability

The database of ^{14}C ages, geochemical and pollen data and graphs and the age model code are available through https://doi.org/10.5281/zenodo.10839531 (Vidaller et al., 2024).

Acknowledgments

This study was supported by the Spanish project PID 2019–106050RB-I00 (PYCACHU) and the Interreg-POCTEFA project OPCC ADAPYR. Ixeia Vidaller is supported by the grant FPU18/04978 and is enrolled in the PhD programme at the University of Zaragoza.

We acknowledge the help of Kilian Jungkeit, Juan Bernal, Marcel Galofré, Inés de la Parra during the field work and Eneko Iriarte (University of Burgos) for providing a vibracorer system. Graciela Gil-Romera is acknowledged for her support with the age-model construction. Thanks are also owed to AEMET for sharing the climatic data of Renclusa hut and to Posets-Maladeta Natural Park for allowing the field work permits necessary to this investigation.

Appendix A. Supplementary material

Supplementary data to this article can be found online at https://doi.org/10.1016/j.catena.2024.108059.

References

Bartolomé, M., Sancho, C., Benito, G., Medialdea, A., Calle, M., Moreno, A., Leunda, M., Luetscher, M., Muñoz, A., Bastida, J., Cheng, H., Edwards, R.L., 2021. Effects of glaciation on karst hydrology and sedimentology during the Last Glacial Cycle: the case of Granito cave, Central Pyrenees (Spain). Catena (amst) 206, 105252. https://doi.org/10.1016/j.catena.2021.105252.

Battarbee, R.W., Jones, V.J., Flower, R.J., Cameron, N.G., Bennion, H., Carvalho, L., Juggins, S., 2001. Diatoms. Springer.

Beniston, M., Farinotti, D., Stoffel, M., Andreassen, L.M., Coppola, E., Eckert, N., Fantini, A., Giacona, F., Hauck, C., Huss, M., Huwald, H., Lehning, M., López-Moreno, J.I., Magnusson, J., Marty, C., Morán-Tejéda, E., Morin, S., Naaim, M., Provenzale, A., Rabatel, A., Six, D., Stötter, J., Strasser, U., Terzago, S., Vincent, C., 2018. The European mountain cryosphere: a review of its current state, trends, and future challenges. Cryosphere 12, 759–794. https://doi.org/10.5194/tc-12-759-2018.

Bennett, K., 2002. Documentation for Psimpoll 4.10 and Pscomb 1.03. C Programs for Plotting Pollen Diagrams and Analysing Pollen Data.

Blaauw, M., Christen, J., 2011. Flexible paleoclimate age-depth models using an autoregressive gamma process. Bayesian Anal 6. https://doi.org/10.1214/ba/1339616472.

Bordonau, J., 1993. The Upper Pleistocene ice-lateral till complex of Cerler (Esera valley, central Southern Pyrenees: Spain). Quat. Int. 18, 5–14. https://doi.org/10.1016/1040-6182(93)90048-K.

Bordonau, J., 1992. Els complexos glacio-lacustres relacionats amb el darrer cicle glacial als Pirineus. Universitat de Barcelona. Departament de Geologia Dinàmica, Geofísica i Paleontologia. doi: 10.1002/(sici)1099-1417(199609/10)11:5<434::aid-jqs262>3.0.co;2-v.

Braithwaite, R.J., Hughes, P.D., 2020. Regional Geography of Glacier Mass Balance Variability Over Seven Decades 1946–2015. Front Earth Sci (Lausanne).

Cacho, I., Grimalt, J.O., Pelejero, C., Canals, M., Sierro, F.J., Flores, J.A., Shackleton, N., 1999. Dansgaard-Oeschger and Heinrich event imprints in Alboran Sea paleotemperatures. Paleoceanography 14, 698–705. https://doi.org/10.1029/1999PA900044.

Cacho, I., Grimalt, J.O., Canals, M., Sbaffi, L., Shackleton, N.J., Schönfeld, J., Zahn, R., 2001. Variability of the western Mediterranean Sea surface temperature during the last 25,000 years and its connection with the Northern Hemisphere climatic changes. Paleoceanography 16, 40–52. https://doi.org/10.1029/2000PA000502.

Calero, M.A., Valero-Garcés, B.L., Rull, V., Vegas-Vilarrúbia, T., Garcés-Pastor, S., López-Vila, J., Camarero, J.J., 2016. El registro sedimentario del lago Sant Maurici (Pirineos Centrales). Geogaceta 59, 11–14.

Catalan, J., Pla-Rabés, S., García, J., Camarero, L., 2014. Air temperature-driven CO2 consumption by rock weathering at short timescales: evidence from a Holocene lake sediment record. Geochim Cosmochim. Acta 136, 67–79. https://doi.org/10.1016/j.gca.2014.04.005.

Chawchai, S., Kylander, M.E., Chabangborn, A., Löwemark, L., Wohlfarth, B., 2016. Testing commonly used X-ray fluorescence core scanning-based proxies for organic-rich lake sediments and peat. Boreas 45, 180–189. https://doi.org/10.1111/bor.12145.

Chueca-Cía, J., Julián-Andrés, A., 2008. Geomorphological map of the alta ribagorza (central pyrenees, spain). J Maps 4, 235–247. https://doi.org/10.4113/jom.2008.1006.

Combourieu Nebout, N., Peyron, O., Dormoy, I., Desprat, S., Beaudouin, C., Kotthoff, U., Marret, F., 2009. Rapid climatic variability in the west Mediterranean during the last 25 000 years from high resolution pollen data. Clim. Past 5, 503–521. https://doi.org/10.5194/cp-5-503-2009.

Copons, R., Bordonau, J., 1997. El último ciclo glaciar (Pleistoceno Superior - Holoceno) en el macizo de la Madaleta (Pirineos Centrales). Revista de la Sociedad Geológica de España.

Copons, R., Parés, J.M., Dinarès-Turell, J., Bordonau, J., 1997. Sampling induced AMS in soft sediments: a case study in Holocene glaciolacustrine rhythmites from Lake Barrancs (Central Pyrenees, Spain). Phys. Chem. Earth 22, 137–141. https://doi.org/10.1016/s0079-1946(97)00091-8.

Crest, Y., Delmas, M., Braucher, R., Gunnell, Y., Calvet, M., 2017. Cirques have growth spurts during deglacial and interglacial periods: Evidence from 10Be and 26Al nuclide inventories in the central and eastern Pyrenees. Geomorphology 278, 60–77. https://doi.org/10.1016/j.geomorph.2016.10.035.

Delmas, M., 2015. The last maximum ice extent and subsequent deglaciation of the Pyrenees: an overview of recent research. Cuadern. Invest. Geogr. 41, 359. https://doi.org/10.18172/cig.2708.

Fletcher, W.J., Sánchez Goñi, M.F., Allen, J.R.M., Cheddadi, R., Combourieu-Nebout, N., Huntley, B., Lawson, I., Londeix, L., Magri, D., Margari, V., Müller, U.C., Naughton, F., Novenko, E., Roucoux, K., Tzedakis, P.C., 2010. Millennial-scale variability during the last glacial in vegetation records from Europe. Quat. Sci. Rev. 29, 2839–2864. https://doi.org/10.1016/j.quascirev.2009.11.015.

García-Ruiz, J.M., Serrano, E., 2022. Chapter 4.3 - The Glaciers of the Central-Western Pyrenees. In: Oliva, M., Palacios, D., Fernández-Fernández, J.M. (Eds.), Iberia, Land of Glaciers. Elsevier, pp. 123–155. doi:10.1016/B978-0-12-821941-6.00007-4.

García-Ruiz, J.M., Bordonau, J., Martinez de Pison, E., Vilaplana, J.M., 1992. Mapa Geomorfológico, Benasque (Huesca), Escala 1:50.000. Geoforma Ediciones.

García-Ruiz, J.M., Valero-Garcés, B.L., Martí-Bono, C., González-Sampériz, P., 2003. Asynchroneity of maximum glacier advances in the central Spanish Pyrenees. J. Quat. Sci. 18, 61–72. https://doi.org/10.1002/jqs.715.

García-Ruiz, J.M., Martí-Bono, C., Peña-Monné, J.L., Sancho, C., Rhodes, E.J., Valero-Garcés, B., González-Sampériz, P., Moreno, A., 2012. Glacial and fluvial deposits in the aragón valley, central-western pyrenees: chronology of the pyrenean late pleistocene glaciers. Geogr. Ann. Ser. B 95, 15–32. https://doi.org/10.1111/j.1468-0459.2012.00478.x.

García-Ruiz, J.M., Martí-Bono, C., Peña-Monné, J.L., Sancho, C., Rhodes, E.J., Valero-Garcés, B., González-Sampériz, P., Moreno, A., 2013. Glacial and fluvial deposits in the Aragón Valley, Central-Western pyrenees: chronology of the pyrenean late pleistocene glaciers. Geogr. Ann. Ser. B 95, 15–32. https://doi.org/10.1111/j.1468-0459.2012.00478.x.

García-Ruiz, J.M., Palacios, D., González-Sampériz, P., de Andrés, N., Moreno, A., Valero-Garcés, B., Gómez-Villar, A., 2016. Mountain glacier evolution in the Iberian Peninsula during the Younger Dryas. Quat. Sci. Rev. 138, 16–30. https://doi.org/10.1016/j.quascirev.2016.02.022.

García-Sansegundo, J., Ramírez-Merino, J.I., Rodríguez-Santisteban, R., Leyva, F., 2013. Mapa Geológico de España, Escala 1:50.000, Hoja 148, Vielha.

Gellatly, A.F., Grove, J.M., Switsur, V.R., 1992. Mid-Holocene glacial activity in the Pyrenees. Holocene 2, 266–270. https://doi.org/10.1177/095968369200200309.

Goeury, C., De Beaulieu, J.L., 1979. À propos de la concentration du pollen à l'aide de la liqueur de Thoulet dans les sédiments minéraux. Pollen et spores 21.

González-Sampériz, P., Valero-Garcés, B.L., Moreno, A., Jalut, G., García-Ruiz, J.M., Martí-Bono, C., Delgado-Huertas, A., Navas, A., Otto, T., Dedoubat, J.J., 2006. Climate variability in the Spanish Pyrenees during the last 30,000 yr revealed by the El Portalet sequence. Quat Res 66, 38–52. https://doi.org/10.1016/j.yqres.2006.02.004.

González-Sampériz, P., Aranbarri, J., Pérez-Sanz, A., Gil-Romera, G., Moreno, A., Leunda, M., Sevilla-Callejo, M., Corella, J.P., Morellón, M., Oliva, B., Valero-Garcés, B., 2017. Environmental and climate change in the southern Central Pyrenees since the Last Glacial Maximum: a view from the lake records. Catena (amst) 149, 668–688. https://doi.org/10.1016/j.catena.2016.07.041.

González-Sampériz, P., Gil-Romera, G., García-Prieto, E., Aranbarri, J., Moreno, A., Morellón, M., Sevilla-Callejo, M., Leunda, M., Santos, L., Franco-Múgica, F., Andrade, A., Carrión, J.S., Valero-Garcés, B.L., 2020. Strong continentality and effective moisture drove unforeseen vegetation dynamics since the last interglacial at inland Mediterranean areas: the Villarquemado sequence in NE Iberia. Quat Sci Rev 242, 106425. https://doi.org/10.1016/j.quascirev.2020.106425.

Greenwood, S.L., Hughes, A.L.C., 2022. Chapter 5 - Glacial landscapes of Fennoscandia. In: Palacios, D., Hughes, P.D., García-Ruiz, J.M., Andrés, N. (Eds.), European Glacial Landscapes. Elsevier, pp. 37–43. doi: doi: 10.1016/B978-0-12-823498-3.00051-0.

Grunewald, K., Scheithauer, J., 2010. Europe's southernmost glaciers: response and adaptation to climate change. J. Glaciol. 56, 129–142. https://doi.org/10.3189/002214310791190947.

Hammer, D.A.T., Ryan, P.D., Hammer, Ø., Harper, D.A.T., 2001. Past: paleontological statistics software package for education and data analysis. Palaeontol. Electron.

Hughes, P.D., 2018. Little ice age glaciers and climate in the mediterranean mountains: a new analysis. Geogr. Res. Lett. 44, 15–45. https://doi.org/10.18172/cig.3362.

Hughes, P.D., Woodward, J.C., 2008. Timing of glaciation in the Mediterranean mountains during the last cold stage. J. Quat. Sci. 23, 575–588. https://doi.org/10.1002/jqs.1212.

Hughes, P.D., Gibbard, P.L., Ehlers, J., 2013. Timing of glaciation during the last glacial cycle: evaluating the concept of a global 'Last Glacial Maximum' (LGM). Earth Sci. Rev. 125, 171–198. https://doi.org/10.1016/j.earscirev.2013.07.003.

Huss, M., Fischer, M., 2016. Sensitivity of Very Small Glaciers in the Swiss Alps to Future Climate Change. Front Earth Sci (Lausanne).

Jalut, G., Delibrias, G., Dagnac, J., Mardones, M., Bouhours, M., 1982. A palaeoecological approach to the last 21 000 years in the pyrenees: the peat bog of Freychinede (alt. 1350 m, Ariege, South France). Palaeogeogr. Palaeoclimatol. Palaeoecol. 40, 321–359. https://doi.org/10.1016/0031-0182(82)90033-5.

Jalut, G., Marti, J.M., Fontugne, M., Delibrias, G., Vilaplana, J.M., Julia, R., 1992. Glacial to interglacial vegetation changes in the northern and southern Pyrénées: deglaciation, vegetation cover and chronology. Quat. Sci. Rev. 11, 449–480. https://doi.org/10.1016/0277-3791(92)90027-6.

Jiménez-Sánchez, M., Rodríguez-Rodríguez, L., García-Ruiz, J.M., Domínguez-Cuesta, M. J., Farias, P., Valero-Garcés, B., Moreno, A., Rico, M., Valcárcel, M., 2013. A review of glacial geomorphology and chronology in northern Spain: timing and regional variability during the last glacial cycle. Geomorphology 196, 50–64. https://doi.org/10.1016/j.geomorph.2012.06.009.

Jomelli, V., Chapron, E., Favier, V., Rinterknecht, V., Braucher, R., Tournier, N., Gascoin, S., Marti, R., Galop, D., Binet, S., Deschamps-Berger, C., Tissoux, H., Aumaitre, G., Bourlès, D.L., Keddadouche, K., 2020. Glacier fluctuations during the Late Glacial and Holocene on the Ariège valley, northern slope of the Pyrenees and reconstructed climatic conditions. Mediterr. Geosci. Rev. 2, 37–51. https://doi.org/10.1007/s42990-020-00018-5.

Juggins, S., 2017. Rioja: Analysis of Quaternary Science Data. R Package Version (9-15), 1.

Krammer, K., Lange-Bertalot, H., 1986. Bacillariophyceae. 1. Teil: Naviculaceae. In: Ettl, H., Gerloff, J., Heynig, H., Mollenhauer, D. (Eds.), Süsswasser Flora von Mitteleuropa.

Krammer, K., Lange-Bertalot, 1988. Bacillariophyceae. 2. Teil: Bacillariaceae, Epithemiaceae, Surirellaceae. In: Ettl, H., Gerloff, J., Heynig, H., Mollenhauer, D. (Eds.), Süsswasserflora VonMitteleuropa.

Krammer, K., Lange-Bertalot, 1991a. Bacillariophyceae. 3. Teil: Centrales, Fragilariaceae, Eunotiaceae. In: Ettl, H., Gerloff, J., Heynig, H., Mollenhauer, D. (Eds.), Süsswasserflora von Mitteleuropa.

Krammer, K., Lange-Bertalot, H., 1991b. Bacillariophyceae. 4. Teil: Achnanthaceae, Kritische Ergänzungen zu Navicula (Lineolatae) und Gomphonema, Gesamtliteraturverzeichnis Teil 1-4. In: Ettl, H., Gätner, G., Gerloff, J., Heynig, H., Mollenhauer, D. (Eds.), Süsswasserflora von Mitteleuropa.

Kwiecien, O., Stockhecke, M., Pickarski, N., Heumann, G., Litt, T., Sturm, M., Anselmetti, F., Kipfer, R., Haug, G.H., 2014. Dynamics of the last four glacial terminations recorded in Lake Van, Turkey. Quat. Sci. Rev. 104, 42–52. https://doi.org/10.1016/j.quascirev.2014.07.001.

Legendre, P., Gallagher, E.D., 2001. Ecologically meaningful transformations for ordination of species data. Oecologia 129, 271–280. https://doi.org/10.1007/s004420100716.

Leonard, E.M., Reasoner, M.A., 1999. A continuous holocene glacial record inferred from proglacial lake sediments in Banff National Park, Alberta, Canada. Quat. Res. 51, 1–13. https://doi.org/10.1006/qres.1998.2009.

Leunda, M., González-Sampériz, P., Gil-Romera, G., Aranbarri, J., Moreno, A., Oliva-Urcia, B., Sevilla-Callejo, M., Valero-Garcés, B., 2017. The Late-Glacial and Holocene Marboré Lake sequence (2612 m a.s.l., Central Pyrenees, Spain): testing high altitude sites sensitivity to millennial scale vegetation and climate variability. Glob Planet Change 157, 214–231. https://doi.org/10.1016/j.gloplacha.2017.08.008.

Lewis, C.J., McDonald, E.V., Sancho, C., Peña, J.L., Rhodes, E.J., 2009. Climatic implications of correlated Upper Pleistocene glacial and fluvial deposits on the Cinca and Gállego Rivers (NE Spain) based on OSL dating and soil stratigraphy. Glob Planet Change 67, 141–152. https://doi.org/10.1016/j.gloplacha.2009.01.001.

Livingstone, S.J., Clark, C.D., Piotrowski, J.A., Tranter, M., Bentley, M.J., Hodson, A., Swift, D.A., Woodward, J., 2012. Theoretical framework and diagnostic criteria for the identification of palaeo-subglacial lakes. Quat. Sci. Rev. 53, 88–110. https://doi.org/10.1016/j.quascirev.2012.08.010.

Livingstone, S.J., Piotrowski, J.A., Bateman, M.D., Ely, J.C., Clark, C.D., 2015. Discriminating between subglacial and proglacial lake sediments: an example from the Dänischer Wohld Peninsula, Northern Germany. Quat. Sci. Rev. 112, 86–108. https://doi.org/10.1016/j.quascirev.2015.01.030.

Livingstone, S.J., Li, Y., Rutishauser, A., Sanderson, R.J., Winter, K., Mikucki, J.A., Björnsson, H., Bowling, J.S., Chu, W., Dow, C.F., Fricker, H.A., McMillan, M., Ng, F. S.L., Ross, N., Siegert, M.J., Siegfried, M., Sole, A.J., 2022. Subglacial lakes and their changing role in a warming climate. Nat Rev Earth Environ 3, 106–124. https://doi.org/10.1038/s43017-021-00246-9.

López-Moreno, J.I., Revuelto, J., Rico, I., Chueca-Cía, J., Julián, A., Serreta, A., Serrano, E., Vicente-Serrano, S.M., Azorin-Molina, C., Alonso-González, E., García-Ruiz, J.M., 2016. Thinning of the Monte Perdido Glacier in the Spanish Pyrenees since 1981. Cryosphere 10, 681–694. https://doi.org/10.5194/tc-10-681-2016.

Lotter, A.F., Birks, H.J.B., Zolitschka, B., 1995. Late-glacial pollen and diatom changes in response to two different environmental perturbations: volcanic eruption and Younger Dryas cooling. J. Paleolimnol. 14, 23–47. https://doi.org/10.1007/BF00682592.

Lotter, A.F., Birks, H.J.B., Hofmann, W., Marchetto, A., 1997. Modern diatom, cladocera, chironomid, and chrysophyte cyst assemblages as quantitative indicators for the reconstruction of past environmental conditions in the Alps. I. Climate. J. Paleolimnol. 18, 395–420. https://doi.org/10.1023/A:1007982008956.

Martí-Bono, C., García-Ruíz, J.M., 1994. El Glaciarismo Surpirenaico: Nuevas Aportaciones. Geoforma Ediciones, Logroño.

Martínez de Pisón, E., 1989. Morfologia glaciar del valle de Benasque. Eria.

Martínez de Pisón, E., 1990. Morfoestructuras del valle de Benasque (Pirineo Aragonés). Anales de geografía de la Universidad Complutense 121–148.

Meyers, P.A., 1997. Organic geochemical proxies of paleoceanographic, paleolimnologic, and paleoclimatic processes. Org. Geochem. 27, 213–250. https://doi.org/10.1016/S0146-6380(97)00049-1.

Miras, Y., Ejarque, A., Riera, S., Palet, J.M., Orengo, H., Euba, I., 2007. Dynamique holocène de la végétation et occupation des Pyrénées andorranes depuis le Néolithique ancien, d'après l'analyse pollinique de la tourbière de Bosc dels Estanyons (2180m, Vall del Madriu, Andorre). C.R. Palevol. 6, 291–300. https://doi.org/10.1016/j.crpv.2007.02.005.

Montserrat Marti, J.M., 1992. Evolución glaciar y postglaciar del clima y la vegetación en la vertiente sur del Pirineo: estudio palinológico. Consejo Superior De Investigaciones Científicas (España).

Moore, P.D., Webb, J.A., Collinson, M.E., 1991. Pollen Analysis. Hodder and Stroughton, London.

Morellón, M., Valero-Garcés, B., Moreno, A., González-Sampériz, P., Mata, P., Romero, O., Maestro, M., Navas, A., 2008. Holocene palaeohydrology and climate variability in northeastern Spain: the sedimentary record of Lake Estanya (Pre-Pyrenean range). Quat. Int. 181, 15–31. https://doi.org/10.1016/j.quaint.2007.02.021.

Morellón, M., Pérez-Sanz, A., Corella, J.P., Büntgen, U., Catalán, J., González-Sampériz, P., González-Trueba, J.J., López-Sáez, J.A., Moreno, A., Pla-Rabes, S., Saz-Sánchez, M.A., Scussolini, P., Serrano, E., Steinhilber, F., Stefanova, V., Vegas-Vilarrúbia, T., Valero-Garcés, B., 2012. A multi-proxy perspective on millennium-long climate variability in the Southern Pyrenees. Clim. Past 8, 683–700. https://doi.org/10.5194/cp-8-683-2012.

Moreno, A., Valero-Garcés, B.L., Jiménez-Sánchez, M., Domínguez-Cuesta, M.J., Mata, M.P., Navas, A., González-Sampériz, P., Stoll, H., Farias, P., Morellón, M., Corella, J.P., Rico, M., 2010. The last deglaciation in the Picos de Europa National Park (Cantabrian Mountains, northern Spain). J. Quat. Sci. 22, 1076–1091. https://doi.org/10.1002/jqs.1265.

Moreno, A., López-Merino, L., Leira, M., Marco-Barba, J., González-Sampériz, P., Valero-Garcés, B.L., López-Sáez, J.A., Santos, L., Mata, P., Ito, E., 2011. Revealing the last 13,500 years of environmental history from the multiproxy record of a mountain lake (Lago Enol, northern Iberian Peninsula). J. Paleolimnol. 46, 327–349. https://doi.org/10.1007/s10933-009-9387-7.

Moreno, A., González-Sampériz, P., Morellón, M., Valero-Garcés, B.L., Fletcher, W.J., 2012. Northern Iberian abrupt climate change dynamics during the last glacial cycle: a view from lacustrine sediments. Quat. Sci. Rev. 36, 139–153. https://doi.org/10.1016/j.quascirev.2010.06.031.

Moreno, A., Svensson, A., Brooks, S.J., Connor, S., Engels, S., Fletcher, W., Genty, D., Heiri, O., Labuhn, I., Perşoiu, A., Peyron, O., Sadori, L., Valero-Garcés, B., Wulf, S., Zanchetta, G., 2014. A compilation of Western European terrestrial records 60–8 ka BP: towards an understanding of latitudinal climatic gradients. Quat. Sci. Rev. 106, 167–185. https://doi.org/10.1016/j.quascirev.2014.06.030.

Moreno, A., Bartolomé, M., López-Moreno, J.I., Pey, J., Corella, J.P., García-Orellana, J., Sancho, C., Leunda, M., Gil-Romera, G., González-Sampériz, P., Pérez-Mejías, C., Navarro, F., Otero-García, J., Lapazaran, J., Alonso-González, E., Cid, C., López-Martínez, J., Oliva-Urcia, B., Faria, S.H., Sierra, M.J., Millán, R., Querol, X., Alastuey, A., García-Ruíz, J.M., 2021. The case of a southern European glacier which survived Roman and medieval warm periods but is disappearing under recent warming. Cryosphere 15, 1157–1172. https://doi.org/10.5194/tc-15-1157-2021.

Ohlendorf, C., Sturm, M., Hausmann, S., 2003. Natural environmental changes and human impact reflected in sediments of a high alpine lake in Switzerland. J. Paleolimnol. 30, 297–306. https://doi.org/10.1023/A:1026032829150.

Oliva, M., Palacios, D., Fernández-Fernández, J.M., Rodríguez-Rodríguez, L., García-Ruiz, J.M., Andrés, N., Carrasco, R.M., Pedraza, J., Pérez-Alberti, A., Valcárcel, M., Hughes, P.D., 2019. Late Quaternary glacial phases in the Iberian Peninsula. Earth Sci. Rev. 192, 564–600. https://doi.org/10.1016/j.earscirev.2019.03.015.

Oliva-Urcía, B., Moreno, A., Leunda, M., Valero-Garcés, B., González-Sampériz, P., Gil-Romera, G., Mata, M.P., Adsuar, A., Aranbarri, J., Barreiro, F., Bartolomé, M., Bueno, B., García-Prieto, E., García, B., Larrasoaña, J.C., Parés, J.M., Pérez, A., Rico, M., Salabarnada, A., Salazar, Á., Sevilla-Callejo, M., Tarrats, P., 2018. Last deglaciation and Holocene environmental change at high altitude in the Pyrenees: the geochemical and paleomagnetic record from Marboré Lake (N Spain). J. Paleolimnol. 59, 349–371. https://doi.org/10.1007/s10933-017-0013-9.

Ollero Ojeda, A., Cadiñanos Aguirre, J., Meaza Rodríguez, G., Ormaetxea Arenaza, O., González Amuchastegui, M., 2001. Medios dinámicos en la cabecera del río Ésera (Pirineo Central). Treballs De La Societat Catalana De Geografia 137–163. https://doi.org/10.2436/tscg.v0i52.37262.

Palacios, D., García-Ruiz, J.M., Andrés, N., Schimmelpfennig, I., Campos, N., Léanni, L., Aumaître, G., Bourlès, D.L., Keddadouche, K., 2017. Deglaciation in the central Pyrenees during the Pleistocene-Holocene transition: timing and geomorphological significance. Quat. Sci. Rev. 162, 111–127. https://doi.org/10.1016/j.quascirev.2017.03.007.

Pallàs, R., Rodés, Á., Braucher, R., Carcaillet, J., Ortuño, M., Bordonau, J., Bourlès, D., Vilaplana, J.M., Masana, E., Santanach, P., 2006. Late Pleistocene and Holocene glaciation in the Pyrenees: a critical review and new evidence from 10Be exposure ages, south-central Pyrenees. Quat. Sci. Rev. 25, 2937–2963. https://doi.org/10.1016/j.quascirev.2006.04.004.

Patton, H., Hubbard, A., Heyman, J., Alexandropoulou, N., Lasabuda, A.P.E., Stroeven, A.P., Hall, A.M., Winsborrow, M., Sugden, D.E., Kleman, J., Andreassen, K., 2022. The extreme yet transient nature of glacial erosion. Nat. Commun. 13, 7377. https://doi.org/10.1038/s41467-022-35072-0.

Pérez-Sanz, A., González-Sampériz, P., Moreno, A., Valero-Garcés, B., Gil-Romera, G., Rieradevall, M., Tarrats, P., Lasheras-Álvarez, L., Morellón, M., Belmonte, A., Sancho, C., Sevilla-Callejo, M., Navas, A., 2013. Holocene climate variability, vegetation dynamics and fire regime in the central Pyrenees: the Basa de la Mora sequence (NE Spain). Quat. Sci. Rev. 73, 149–169. https://doi.org/10.1016/j.quascirev.2013.05.010.

Pla, S., Catalan, J., 2005. Chrysophyte cysts from lake sediments reveal the submillennial winter/spring climate variability in the northwestern Mediterranean region throughout the Holocene. Clim. Dyn. 24, 263–278. https://doi.org/10.1007/s00382-004-0482-1.

Rasmussen, S.O., Bigler, M., Blockley, S.P., Blunier, T., Buchardt, S.L., Clausen, H.B., Cvijanovic, I., Dahl-Jensen, D., Johnsen, S.J., Fischer, H., Gkinis, V., Guillevic, M., Hoek, W.Z., Lowe, J.J., Pedro, J.B., Popp, T., Seierstad, I.K., Steffensen, J.P., Svensson, A.M., Vallelonga, P., Vinther, B.M., Walker, M.J.C., Wheatley, J.J., Winstrup, M., 2014. A stratigraphic framework for abrupt climatic changes during the Last Glacial period based on three synchronized Greenland ice-core records: refining and extending the INTIMATE event stratigraphy. Quat. Sci. Rev. 106, 14–28. https://doi.org/10.1016/j.quascirev.2014.09.007.

Reille, M., Lowe, J.J., 1993. A re-evaluation of the vegetation history of the eastern Pyrenees (France) from the end of the last glacial to the present. Quat. Sci. Rev. 12, 47–77. https://doi.org/10.1016/0277-3791(93)90048-Q.

Reimer, P.J., Austin, W.E.N., Bard, E., Bayliss, A., Blackwell, P.G., Bronk Ramsey, C., Butzin, M., Cheng, H., Edwards, R.L., Friedrich, M., Grootes, P.M., Guilderson, T.P., Hajdas, I., Heaton, T.J., Hogg, A.G., Hughen, K.A., Kromer, B., Manning, S.W., Muscheler, R., Palmer, J.G., Pearson, C., Van Der Plicht, J., Reimer, R.W., Richards, D.A., Scott, E.M., Southon, J.R., Turney, C.S.M., Wacker, L., Adolphi, F., Büntgen, U., Capano, M., Fahrni, S.M., Fogtmann-Schulz, A., Friedrich, R., Köhler, P., Kudsk, S., Miyake, F., Olsen, J., Reinig, F., Sakamoto, M., Sookdeo, A., Talamo, S., 2020. The IntCal20 Northern Hemisphere Radiocarbon Age Calibration Curve (0–55 cal kBP). Radiocarbon 62, 725–757. https://doi.org/10.1017/RDC.2020.41.

Reixach, T., 2022. Chronologie des fluctuations glaciaires dans les Pyrénées au cours du Pléistocène supérieur - implications paléoclimatiques. Universite De Perpignan Via Domitia, Perpignan.

Rico, I., Izagirre, E., Serrano, E., López-Moreno, J.I., 2017. Superficie glaciar actual en los Pirineos: una actualización para 2016. Pirineos 172, e029.

Ríos-Aragüés, L.M., Galera Fernández, J.M., Barettino Fraile, D., Charlet, J.M., 2002. Mapa Geológico de Epaña, Escala 1:50.000, Hoja 180, Benasque.

Rivera Rondón, C.A., Catalan, J., 2017. Diatom diversity in the lakes of the Pyrenees: an iconographic reference. Limnetica 29, 127–395. https://doi.org/10.23818/limn.36.10.

Salazar-Rincón, A., Mata-Campo, P., Rico-Herrero, M.T., Valero-Garcés, B.L., Oliva-Urcia, B., Ibarra, P., Rubio, F.M., Horda, G., Adsuar, A., Aranbarri, J., Barreiro, F., Bartolomé, M., Bueno, B., García-Prieto, E., García, B., Gil, G., González, P., Larrasoaña, J.C., Parés, J.M., Pérez, A., Rico, M., Salabarnada, A., Salazar, Á., Sevilla-Callejo, M., Tarrats, P., 2013. The paleolake of La Larri (Pineta valley, Pyrenees): explanation in the framework of the last glacial maximum in the Pyrenees. Cuadern. Invest. Geogr. 39, 97–116.

Sancho, C., Arenas, C., Pardo, G., Peña-Monné, J.L., Rhodes, E.J., Bartolomé, M., García-Ruiz, J.M., Martí-Bono, C., 2018. Glaciolacustrine deposits formed in an ice-dammed tributary valley in the south-central Pyrenees: new evidence for late Pleistocene climate. Sediment. Geol. 366, 47–66. https://doi.org/10.1016/j.sedgeo.2018.01.008.

Schnurrenberger, D., Russell, J., Kelts, K., 2003. Classification of lacustrine sediments based on sedimentary components. J. Paleolimnol. 29, 141–154. https://doi.org/10.1023/A:1023270324800.

Serrano, E., de Sanjosé-Blasco, J.J., Gómez-Lende, M., López-Moreno, J.I., Pisabarro, A., Martínez-Fernández, A., 2019. Periglacial environments and frozen ground in the central Pyrenean high mountain area: ground thermal regime and distribution of landforms and processes. Permafr. Periglac. Process 30, 292–309. https://doi.org/10.1002/ppp.2032.

Smol, J., 2011. Paleophycology of a high Arctic lake near Cape Herschel, Ellesmere Island. Can. J. Bot. 61, 2195–2204. https://doi.org/10.1139/b83-238.

Stockmarr, J., 1971. Tablets with spores used in absolute pollen analysis. Pollen Spores 13, 615–621.

Vidaller, I., Revuelto, J., Izagirre, E., Rojas-Heredia, F., Alonso-González, E., Gascoin, S., René, P., Berthier, E., Rico, I., Moreno, A., Serrano, E., Serreta, A., López-Moreno, J. I., 2021. Toward an ice-free mountain range: demise of pyrenean glaciers during 2011–2020. Geophys Res Lett 48. https://doi.org/10.1029/2021GL094339.

Vidaller, I., Izagirre, E., Del Río, L.M., Alonso-González, E., Rojas-Heredia, F., Serrano, E., Moreno, A., López-Moreno, J.I., Revuelto, J., 2023. The Aneto Glacier (Central Pyrenees) evolution from 1981 to 2022: ice loss observed from historic aerial image photogrammetry and remote sensing techniques. Cryosphere.

Villar, L., Sesé, J.A., Ferrández, J.V., 2001. Atlas de la Flora del Pirineo Aragonés, Instituto. ed. Ediciones La Val de Onsera, Spain.

Wu, L., Wilson, D.J., Wang, R., Yin, X., Chen, Z., Xiao, W., Huang, M., 2020. Evaluating Zr/Rb ratio from XRF scanning as an indicator of grain-size variations of glaciomarine sediments in the southern ocean. Geochem. Geophys. Geosyst. 21 https://doi.org/10.1029/2020GC009350.